

Bachelor's Thesis

# Top Antitop Production at LHC

Submitted by

Kilian Trüten

September 19, 2025

First Examiner: PD. Dr. Karol Kovařík

Second Examiner: Dr. Tomáš Ježo

University of Münster Institute for Theoretical Physics

## Contents

1	Introduction			2
<b>2</b>	Theoretical Background			3
	2.1 Constituents of the Proton			3
	2.2 Gauge Theory			4
	2.3 QCD Feynman Rules			6
	2.4 Cross Section			8
	2.5 Monte Carlo Integration	. <b>.</b>		9
	2.5.1 Hit-or-Miss Monte Carlo			10
3	Kinematics			10
4	Calculation of the Squared Matrix Element			14
	4.1 S-Channel			15
	4.2 T-Channel			16
	4.3 U-Channel			18
	4.4 Cross-Channels			18
5	Numerical Evaluation			20
	5.1 Integration Bounds			20
	5.2 Generating Integration Variables			20
	5.3 Cuts			
	5.4 Evaluation of the Hadronic Cross Section			24
	5.5 Differential Cross Sections			26
6	Conclusion & Outlook			29
$\mathbf{A}$	A Appendix			30

## 1 Introduction

The aim of this work is to learn about the working methods of theoretical particle physics by investigating top–antitop production in proton-proton collisions at the LHC at  $\sqrt{s}=8\,\mathrm{TeV}$ . We provide a clear illustration of the leading order calculation of the  $t\bar{t}$  production cross section (CS) and normalized differential cross section and compare the predictions with experimental data from the CMS collaboration. Although the calculation is limited to leading order and to the gluon–gluon channel, we find that the CS only has a relative deviation of about 25% to experimental data and the normalized differential CS successfully predicts the general shape of the bins. This forms the foundation for future analyses at higher orders.

The top quark, discovered in 1995 at Fermilab, is the heaviest known elementary particle in the Standard Model of particle physics. With a mass close to the electroweak symmetry breaking scale, it plays a special role in precision tests of the Standard Model and in searches for new physics [3]. Due to its extremely short lifetime  $\approx 10^{-25}$  s [8], the top quark decays before hadronization occurs, which allows direct access to its properties. Measurements of top quark production and decay therefore provide valuable insights into strong interactions at high energies. At the Large Hadron Collider (LHC), Top Antitop  $(t\bar{t})$  pairs are predominantly produced in proton–proton collisions. The study of  $t\bar{t}$  production cross sections is of particular importance. On the one hand, it provides stringent tests of Quantum Chromodynamics (QCD), on the other hand, it serves as a background to many searches for physics beyond the Standard Model.

In this thesis, the hadronic CS of  $t\bar{t}$  production at a center-of-mass energy  $\sqrt{s}=8\,\mathrm{TeV}$  is calculated at leading order (LO), considering only the gluon–gluon fusion process. A set of equally and random logarithmic distributed events is created and shaped to align with experimental limitations. The calculation is then performed using the Monte Carlo method, which allows an efficient evaluation of the multidimensional phase space integrals involved. Based on this result, a set of unweighted events is generated and stored in the Les Houches Event (LHE) format. From these events, two normalized differential cross sections are extracted and compared with experimental data.

In chapter 2 an overview of the theoretical framework is given, introducing the proton and the transition from hadrons to partons, where the parton distribution functions (PDFs) and the momentum fractions x are established. A short overview of Quantum Chromodynamics is given, from which the Feynman rules are motivated. We then take a further look at the kinematics of the process and establish the hadronic CS

$$\sigma_{had} = \sum_{i,j,k,l} \int \int dx_1 dx_2 f_i(x_1, Q^2) f_j(x_2, Q^2) \int dPS_2 \frac{1}{F} |\overline{M(ij \to kl)}|^2,$$

which quantifies the likelihood of a scattering event. The main components are the PDFs  $f_i(x, Q^2)$ , the phase space element dPS<sub>2</sub> and the squared matrix element  $|M|^2$ . These are analytically calculated, partially using Mathematica, and the integration is performed using the Monte Carlo (MC) method.

## 2 Theoretical Background

Proton–proton interactions are studied at the Large Hardron Collider, where hadron beams collide in order to examine the structure of the hadrons. The Standard Model summarizes the current knowledge of the basic constituents of matter and their interactions. It is a is a non-abelian gauge theory with the symmetry group  $U(1)\times SU(2)\times SU(3)$  and has a total of twelve gauge bosons: the photon, three weak bosons and eight gluons. A gauge theory is a field theory where the Lagrangian is invariant under transformations according to certain Lie Groups. The color group SU(3) describes strong interactions and the  $SU(2)\times U(1)$  groups describe the electroweak interaction [11]. Quantum Chromodynamics is the theoretical framework for describing strong interactions, which describes the binding of the quarks inside the hadrons. Gluons are the exchange particles of the color field that bind quarks in nucleons and also nucleons into nuclei, and since they carry a color charge, they can directly interact with other gluons. Quarks interact by exchanging color through gluon interaction. Due to color confinement hadrons can only be observed colorless [10]. As usual in particle physics we use natural units and set the speed of light and the reduced planck constant to one:

$$c = 1 \qquad \hbar = 1 \tag{2.1}$$

In the following sections we will give a short introduction to the theoretical framework used in the calculations, establish the Feynman rules and introduce the Monte Carlo integration used for numerical evaluation.

#### 2.1 Constituents of the Proton

The proton is no elementary particle but consists of smaller components called quarks. A Proton consists of three valence quarks, two up quarks and one down quark  $(u_v u_v d_v)$ , accompanied by many quark-antiquark pairs  $u_s \bar{u}_s$ ,  $d_s \bar{d}_s$ ,  $s_s \bar{s}_s$ , and so on, which are known as sea quarks [10]. Their quantum numbers always sum to zero, therefore not changing the quantum numbers of the proton. Protons also consist of gluons, who carry a substantial fraction of the proton's momentum.

If one looks at the proton in a fast moving system, as one would do in proton collisions at the LHC, then the transverse momenta and the rest masses of the proton constituents can be neglected. The structure of the proton is then given to a first approximation by the longitudinal momenta of its constituents. This is the basis of the parton model of Feynman and Bjorken. The constituents of the proton are called partons [18]. Each parton can carry a different fraction x of the parent protons momentum and energy

$$p_{parton} = x p_{proton} , (2.2)$$

where  $P_{proton} = |p|(1,0,0,1)$  is the four momentum of a proton moving along the z-axis. The parton distribution function (PDF)  $f_i(x,Q^2)$  describes the probability that the parton i carries a fraction  $x \in [0,1]$  of the protons momentum p at a given energy scale  $Q^2$ . All parton momentum need to add up to one [10, p. 191]

$$\sum_{i} \int dx \, x f_i(x, Q^2) = 1.$$
 (2.3)

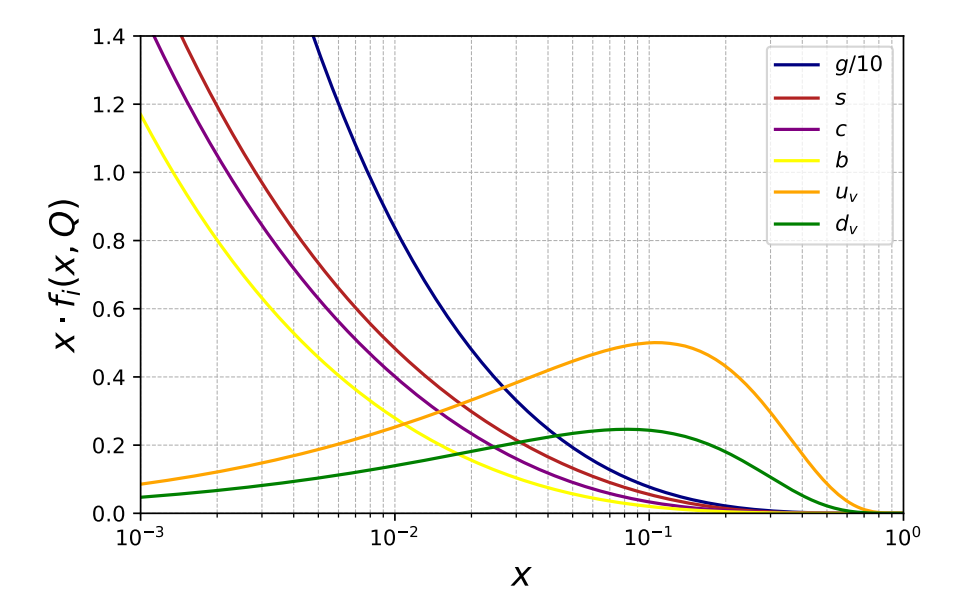


Figure 1: Parton distribution function at engery scale  $Q = 2m_t$ . The used PDF is the "CT18NLO" set [4].

The energy scale for this process is set to two top quark masses  $Q=2m_t$ . Figure 1 displays the used PDF set "CT18NLO" [4] at the set energy scale. The  $u_v$  and  $d_v$  display the up and down valence quarks, calculated by subtracting the anti-quark- from the quark-distribution respectively. The gluon distribution is scaled by 0.1 to allow for better visibility. One can see that it is dominant for small x values, especially for values  $x < 10^{-2}$ . For  $x \approx 10^{-1}$ , the valence quarks carry the significant amount of the protons momentum. Because sea quarks are produced through gluon splitting, they arise for small x values, for larger x values they only carry small amounts of the momentum. The collision under consideration takes place at  $\sqrt{s}=8\,\text{TeV}$ , in comparison the combined mass of the top- anti-top quark is  $m=345\,\text{GeV}$ , where we use the mass of the top quark  $m_t=172.5\,\text{GeV}$ . This implies that small x contribute dominantly to this process, which is why only gluon–gluon fusion is considered.

#### 2.2 Gauge Theory

The following section is based on the work in [19] and [15]. All elementary particle interactions can be described with gauge theories. The three fundamental forces described by the standard model: the electromagnetic, the weak and the strong force, are described by gauge theories that correspond to the symmetry groups U(1), SU(2) and SU(3). The Lagrangian formalism is introduced as a framework, with the Lagrangian as a Lorentz invariant scalar. In classical theories, we describe the physical system in terms of positions of particles depending on time.

$$\mathcal{L} = \mathcal{L}(\vec{q}, \dot{\vec{q}}, t) \tag{2.4}$$

In field theories, fields are used to describe the physical system, the big advantage being they treat space and time equally. The transition is achieved by introducing a Lagrangian density

$$\mathcal{L} = \mathcal{L}(\Phi, \partial_{\mu}\Phi) \tag{2.5}$$

connected to the Lagrangian via  $\mathcal{L} = \int d^3x \,\mathcal{L}$ , where  $\mathcal{L}$  is a function of the field  $\Phi$  and its derivatives  $\partial_{\mu}\Phi$ . The correct field configurations follow from the Euler-Lagrange equation using Fermat's principle, where we find a minimum of the action

$$S = \int \mathcal{L} dt = \int \mathcal{L} d^4x.$$
 (2.6)

We will be guided to the correct form of the Lagrangians by gauge symmetries. For free spin  $\frac{1}{2}$  fields/particles, the equation of motion is given by the Dirac equation with the Dirac Lagrangian

$$\mathcal{L}_{\text{Dirac}} = \bar{\Psi}(i\gamma^{\mu}\partial_{\mu} - m)\Psi \tag{2.7}$$

$$(i\gamma_{\mu}\partial^{\mu} - m)\Psi = 0 \tag{2.8}$$

Because we look at strong interactions, we need to look at the symmetry group SU(3). For this purpose, triplet objects  $Q(x) = (q_1(x), q_2(x), q_3(x))$  are introduced, that are transformed by SU(3) transformations. They contain three spin 1/2 fields, which are interpreted as quarks carrying different color. Because the Lagrangian

$$\mathcal{L} = i\bar{Q}\partial_{\mu}\gamma^{\mu}Q - \bar{Q}mQ \tag{2.9}$$

needs to be locally SU(3) invariant

$$Q(x) \to U(x)Q(x)$$
  $U(x) = e^{iT_a\Theta_a(x)}$ , (2.10)

we need to introduce the covariant derivative

$$D_{\mu} = \partial_{\mu} - ig_s T^a G_{\mu}^a = \partial_{\mu} - ig_s \mathcal{G}_{\mu} , \qquad (2.11)$$

where  $g_s = \sqrt{4\pi\alpha_s}$  is the strong coupling constant,  $T^a$  are the generators of SU(3), which will be introduced below, and  $G^a_{\mu}$  is a gluon field. The gluon field strength tensor  $\mathcal{G}_{\alpha\beta}$  for the spin 1 gluon fields is defined as:

$$\mathcal{G}_{\alpha\beta} = \partial_{\alpha}\mathcal{G}_{\beta} - \partial_{\beta}\mathcal{G}_{\alpha} - g_{s}[\mathcal{G}_{\alpha}, \mathcal{G}_{\beta}]. \tag{2.12}$$

The Lagrangian of QCD can now be quoted as

$$\mathcal{L}_{QCD} = \bar{Q}(iD_{\mu}\gamma^{\mu} - m)Q - \frac{1}{4}\mathcal{G}_{\alpha\beta}\mathcal{G}^{\alpha\beta}. \tag{2.13}$$

SU(3) is the group of all unitary  $3 \times 3$  matrices with

$$U^{\dagger}U = 1 \quad \det(U) = 1.$$
 (2.14)

As usual with Lie groups, these matrices can be written as exponential functions

$$U = e^{iT_a\Theta_a}, (2.15)$$

where the generators are required to be Hermitian and traceless

$$T_a^{\dagger} = T_a \quad \text{Tr}(T_a) = 0. \tag{2.16}$$

In general, a color gauge group SU(N) has  $N^2 - 1$  hermitian generators which can be represented by N×N matrices. For N=3 the generators are related to the Gell-Mann matrices  $\lambda^a$ 

$$(T^a)_{ij} = \frac{\lambda_{ij}^a}{2} \,. \tag{2.17}$$

The Lie algebra is defined by the commutation relation

$$[T^a, T^b] = if^{abc}T^c (2.18)$$

where the letters a,b and c can take on a value from 1 to 8 and  $f^{abc}$  are the fully anti-symmetric structure constants of the SU(3) group with the normalization

$$\operatorname{Tr}\left(T^{a}T^{b}\right) = T_{F}\delta_{ab} \quad T_{F} = \frac{1}{2}.$$
 (2.19)

The color matrices follow a range of rules, the ones relevant for calculating the color terms in the squared matrix element later on are listed below.

$$\sum_{a,k} T_{ik}^a T_{kj}^a = C_F \delta_{ij} \quad C_F = \frac{N^2 - 1}{2N}$$

$$\sum_{cd} f_{acd} f_{bcd} = T_A \delta_{ab} \quad T_A = N$$

$$\sum_{a} T_{ij}^a T_{kl}^a = \frac{1}{2} \left( \delta_{il} \delta_{jk} - \frac{1}{N} \delta_{ij} \delta_{kl} \right)$$
(2.20)

## 2.3 QCD Feynman Rules

The QCD Feynman rules for vertices can be read off the Lagrangian in eq. 2.13 when relations 2.11 and 2.12 are plugged in and fully expanded. One term includes kinetic energy and mass terms and the next three terms give a fermion-fermion-gluon vertex and triple and quadruple gluon vertices [9].

A Feynman diagram represents a perturbative contribution to the amplitude of a quantum transition from some initial quantum state to some final quantum state. Spin- $\frac{1}{2}$ -particles, i.e. quarks and leptons, are represented by straight lines. Gluons are represented by curly lines. External lines represent real particles, either incoming or outgoing, where the arrows on fermion lines are used to distinguish particles from antiparticles: The arrow on the fermion line points forward in time for particles and opposite to the time direction for antiparticles. Each particle has a superscript indicating its spin. The following table show the terms that derive from incoming and outgoing spin- $\frac{1}{2}$ - and spin-1-particles:

where u(p) and v(p) are spinors with four components, which satisfy the completeness relations

$$\sum_{s} u_{a}^{s}(p)\bar{u}_{b}^{s}(p) = (\not p + m)_{ab},$$

$$\sum_{s} v_{a}^{s}(p)\bar{v}_{b}^{s}(p) = (\not p - m)_{ab}.$$
(2.22)

Here the Feynman slash notation is introduced:

$$p \equiv p_{\mu} \gamma^{\mu}. \tag{2.23}$$

The adjungate spinors are calculated via the dirac matrix

$$\bar{u}(p) = u^{\dagger}(p)\gamma^0. \tag{2.24}$$

We denote  $e^{\lambda}(p)$  as the polarization vector of a gluon. While massive spin-1-particles have three polarization states, massless gauge bosons like the gluon have only two polarization states because gauge invariance requires the field polarization to be transverse to the direction that the gluon is traveling. We set the direction of movement to the z-axis, the polarization must be orthogonal to the direction of movement. Summing over all polarization states of the gluons we get [16, p. 59]

$$\sum_{\lambda} \epsilon_{\alpha}^{\lambda} \epsilon_{\beta}^{\lambda \star} = -g_{\alpha\beta} + \frac{p_{\alpha} \bar{p}_{\beta} + p_{\beta} \bar{p}_{\alpha}}{p \cdot \bar{p}}, \qquad (2.25)$$

where we define the momentum vectors of the massless gluons as  $p = (p_0, 0, 0, p_0)$  and  $\bar{p} = (p_0, 0, 0, -p_0)$ .

A vertex represents a point of interaction, the strength of it is denoted by  $g_s$  for strong interaction. The momentum is conserved at each vertex. For the calculations, quark and gluon propagators have to be considered, both can be motivated through the Lagrangian. The quark propagator derives from a coupling between a quark and an anti quark in the Lagrangian, which leads to the Feynman rule for the propagator between two quarks with color i and j

$$q_i \xrightarrow{p} q_j = \frac{i(\not p + m)}{p^2 - m^2} \delta_{ij}. \tag{2.26}$$

The Feynman rule for the gluon propagator <sup>1</sup> is

$$a, \alpha \xrightarrow{p} b, \beta = \frac{-ig^{\alpha\beta}\delta^{ab}}{p^2}, \qquad (2.27)$$

where a and b indicate the color. The delta functions ensure color conservation.

The quark gluon vertex represents the coupling of a gluon to a quark line, the strong coupling constant  $g_s$  indicates the strength of the interaction and the generator  $T_{ij}^a$  encodes the color structure of all particles.

$$G^a_{\mu} = -ig_s T^a_{ij} \gamma_{\mu}$$

$$q_j$$

$$(2.28)$$

Because gluons can interact with each other, three- and four-gluon vertices follow from the Lagrangian, where only the first is relevant for this calculation:

$$G_{\gamma}^{c}$$

$$g_{3}$$

$$g_{3}$$

$$g_{4}$$

$$g_{5}$$

$$g_{6}$$

$$g_{7}$$

#### 2.4 Cross Section

Experimental results on  $2 \to 2$  scattering is usually quoted in terms of a cross section. A cross section  $\sigma$  may be regarded as the effective area over which the particles interact to produce the final state [10]. The hadronic cross section for this process can be written as:

$$\sigma_{had} = \sum_{i,j,k,l} \int \int dx_1 dx_2 f_i(x_1) f_j(x_2) \sigma_{(ij \to kl)}, \qquad (2.30)$$

where the partonic cross section is given by

$$\sigma_{(ij \to kl)} = \int dP S_2 \frac{1}{F} \overline{|M(ij \to kl)|^2}.$$
 (2.31)

The partonic cross section includes the incident flux F, the squared matrix element  $|M(ij \to kl)|^2$  averaged over the spins and the space space element dPS<sub>2</sub>:

$$dPS_2 = \frac{d^3 \vec{k}_1}{(2\pi)^3} \frac{1}{2E_1} \frac{d^3 \vec{k}_2}{(2\pi)^3} \frac{1}{2E_2} (2\pi)^4 \delta^{(4)}(p_1 + p_2 - k_1 - k_2).$$
 (2.32)

<sup>&</sup>lt;sup>1</sup>Only in Feynman gauge, one would get an extra term in axial gauge

To calculate this cross section, we first look at the kinematics of the scattering process, after which we will further simplify the phase space element and determine the flux factor. After that the squared matrix element will be calculated in detail, so that the hadronic cross section can be calculated numerically using the Monte Carlo method. Finally, we will use the Hit or Miss Monte Carlo method to generate unweighted LHE-format events, which will be used to compute differential cross sections and compare those to experimental data in [7].

#### 2.5 Monte Carlo Integration

In many problems of theoretical particle physics, one is faced with the task of evaluating multi-dimensional integrals, for example when computing cross sections or phase space averages. For high-dimensional integrals, deterministic numerical methods become inefficient, and Monte Carlo (MC) techniques provide a powerful alternative. The following description is based on [17].

The central observation of Monte Carlo integration is that an integral can be recast as an average of the integrand. Consider the one-dimensional case,

$$I = \int_{x_1}^{x_2} f(x) dx = (x_2 - x_1) \langle f(x) \rangle, \qquad (2.33)$$

where  $\langle f(x) \rangle$  denotes the average value of f(x) over the interval  $[x_1, x_2]$ . If we generate N random samples  $x_i$  uniformly distributed in  $(x_1, x_2)$ , then the integral can be approximated as

$$I \approx (x_2 - x_1) \frac{1}{N} \sum_{i=1}^{N} f(x_i)$$
 (2.34)

The random sampling ensures that, in the limit of large N, this estimate converges to the exact value of the integral.

The accuracy of the Monte Carlo estimate can be understood using the Central Limit Theorem. The distribution of the average  $\langle f(x) \rangle$  tends to a Gaussian with a standard deviation that scales as

$$\sigma_{\rm MC} = \frac{\sigma}{\sqrt{N}}, \qquad (2.35)$$

where  $\sigma$  is the standard deviation of f(x) with respect to the uniform distribution. Hence, the uncertainty decreases only as  $1/\sqrt{N}$ , which is slower than for deterministic quadrature methods in low dimensions, but crucially independent of the dimensionality of the integral. For convenience, one often introduces the weights  $W_i = (x_2 - x_1) f(x_i)$ , so that the Monte Carlo estimate becomes

$$I \approx I_N = \frac{1}{N} \sum_{i=1}^{N} W_i$$
. (2.36)

The variance can be defined as

$$V_N \equiv \sigma^2 = \frac{1}{N} \sum_{i=1}^N W_i^2 - \left(\frac{1}{N} \sum_{i=1}^N W_i\right)^2.$$
 (2.37)

From this, the Monte Carlo error estimate follows as

$$\sigma_{\rm MC} = \sqrt{\frac{V_N}{N}} \,. \tag{2.38}$$

Thus, the final result for the integral can be written as

$$I \approx I_N \pm \sigma_{\rm MC}$$
. (2.39)

#### 2.5.1 Hit-or-Miss Monte Carlo

In addition to weighted Monte Carlo integration, an alternative approach often used in event generators is the so-called Hit-or-Miss method. The main idea is to generate unweighted events, which is advantageous when simulating realistic experimental data where each event should carry equal importance.

The procedure can be summarized as follows. Suppose we want to integrate a function f(x) over some domain. We first determine the maximum value  $f_{\text{max}}$  of the integrand within the integration region. For each randomly generated point  $x_i$ , we generate a random number  $r_i \in (0,1)$ . The point is then accepted if

$$\frac{f(x_i)}{f_{\text{max}}} > r_i \,, \tag{2.40}$$

and rejected otherwise. Accepted points are assigned equal weight, corresponding to the "hits", while rejected points correspond to the "misses".

### 3 Kinematics

In this chapter we layout the kinematics of the process and derive a term for the phase space element dPS<sub>2</sub>. The kinematics are based on the calculations performed in [14]. We denote the four momenta of the two hadrons with  $P_A$  and  $P_B$ . In the hadronic center of mass frame, the momenta are equal and opposite to each other with  $\vec{P}_A = -\vec{P}_B$  and  $E_A = E_B$ . This leads to the hadronic Mandelstamm variable  $S = (P_A + P_B)^2 = 4E_A^2$ . The four momenta of the partons are

$$p_1 = x_1 P_A \quad p_2 = x_2 P_B \tag{3.1}$$

where both hadrons and partons are assumed to be massless.  $x_1$  and  $x_2$  are momentum fractions that specify what fraction x of the parent protons momentum and energy each parton carries. We define the partonic CM frame by  $\vec{p}_1 + \vec{p}_2 = 0$ . In the hadronic CM frame we get

$$(p_1 + p_2)_{hadr} = \left( (x_1 + x_2)E_A, (x_1 - x_2)\vec{P}_A \right), \tag{3.2}$$

which shows that the partonic CM frame is moving with the velocity of

$$\beta = \frac{|\vec{p}_1 + \vec{p}_2|}{|p_1^0 + p_2^0|} = \frac{x_1 - x_2}{x_1 + x_2} \quad \text{with} \quad E_A = |\vec{P}_A|. \tag{3.3}$$

Since the collision takes place on a parton level, we define the four momenta of the incoming partons as  $p_1$  and  $p_2$  and the four momenta of the outgoing quarks as  $k_1$  and  $k_2$  with the scattering angle  $\theta$  as can be seen in figure 2.

$$p_1 = E_{p_1} \begin{pmatrix} 1 \\ \vec{e}_z \end{pmatrix} \qquad p_2 = E_{p_2} \begin{pmatrix} 1 \\ -\vec{e}_z \end{pmatrix}$$
 (3.4)

$$k_{1} = \begin{pmatrix} E_{k_{1}} \\ \sqrt{E_{k_{1}}^{2} - m_{t}^{2}} \vec{k} \end{pmatrix} \qquad k_{2} = \begin{pmatrix} E_{k_{2}} \\ -\sqrt{E_{k_{2}}^{2} - m_{t}^{2}} \vec{k} \end{pmatrix} \quad \vec{k} = \begin{pmatrix} \sin \theta \\ 0 \\ \cos \theta \end{pmatrix}$$
(3.5)

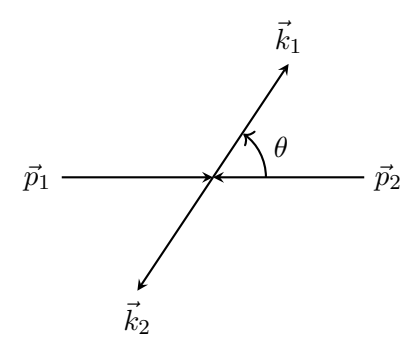


Figure 2: Schematic visualisation of the scattering process in the partonic CM frame defining the scattering angel  $\theta$ .

The distribution of the angle  $\varphi$  is isotropic for this process, therefore it is only implicitly included. Using the energy momentum relation  $E = \sqrt{\vec{k}^2 - m^2}$  and acknowledging the conservation of momentum and energy, one can show that all energies are equal:

$$E_{k_1} = E_{k_2} = E_{p_1} = E_{p_2} = E.$$
 (3.6)

Because these four momentum vectors are defined in the partonic CM system, the momenta in the hadronic system can be calculated using a Lorentz transformation along the z-axis. Because of this the scattering process is described in terms of the Lorentz invariant Mandelstamm variables:

$$s := (p_1 + p_2)^2 = (k_1 + k_2)^2 = x_1 x_2 S$$
(3.7)

$$t := (p_1 - k_1)^2 = (p_2 - k_2)^2 (3.8)$$

$$u := (p_1 - k_2)^2 = (p_2 - k_1)^2, (3.9)$$

with  $\sqrt{s} = 2E$  being the center of mass energy. The Mandelstamm variables are related through the sum of the squared masses

$$s + t + u = m_{p_1}^2 + m_{p_2}^2 + m_{k_1}^2 + m_{k_2}^2 = 2m_t^2. (3.10)$$

We can write the variables t and u in terms of the scattering angle  $\theta$ , which will play a vital role when calculating the cross section:

$$t = p_1^2 + k_1^2 - 2p_1 \cdot k_1$$

$$= m_t^2 - 2\left(E^2 - E\sqrt{E^2 - m_t^2}\cos\theta\right)$$

$$= m_t^2 - \frac{s}{2}\left(1 - \sqrt{1 - \frac{4m_t^2}{s}}\cos\theta\right),$$

$$u = 2m_t^2 - s - t$$

$$= m_t^2 - \frac{s}{2}\left(1 + \sqrt{1 - \frac{4m_t^2}{s}}\cos\theta\right).$$
(3.11)

Now that the kinematic framework is set up, we again focus on the hadronic cross section (eq. 2.30), particularly on the phase space element

$$dPS_2 = \frac{d^3\vec{k}_1}{(2\pi)^3} \frac{1}{2E_1} \frac{d^3\vec{k}_2}{(2\pi)^3} \frac{1}{2E_2} (2\pi)^4 \delta^{(4)}(p_1 + p_2 - k_1 - k_2),$$

which can be further simplified. We start by addressing the integration over the momenta by using the delta function  $\delta(k_1^2 - m_t^2)$  as follows:

$$\begin{split} \frac{\mathrm{d}^4 k_1}{(2\pi)^3} \delta(k_1^2 - m_t^2) &= \frac{\mathrm{d} E_1 \, \mathrm{d}^3 \vec{k}_1}{(2\pi)^3} \delta(E_1^2 - \vec{k}_1^2 - m_t^2) \\ &= \frac{\mathrm{d} E_1 \, \mathrm{d}^3 \vec{k}_1}{(2\pi)^3} \frac{1}{2|E_1|} \Big( \delta(\sqrt{\vec{k}_1^2 + m_t^2} - E_1) + \delta(\sqrt{\vec{k}_1^2 + m_t^2} + E_1) \Big) \,. \end{split}$$

Integrating over the energy and taking into account that the energy can only be positive we get:

$$\frac{\mathrm{d}^{3}\vec{k}_{1}}{(2\pi)^{3}} \int_{-\infty}^{\infty} \frac{\mathrm{d}E_{1}}{2|E_{1}|} \left( \delta(\sqrt{\vec{k}_{1}^{2} + m_{t}^{2}} - E_{1}) + \delta(\sqrt{\vec{k}_{1}^{2} + m_{t}^{2}} + E_{1}) \right) \Theta(E_{1}) = \frac{\mathrm{d}^{3}\vec{k}_{1}}{(2\pi)^{3}} \frac{1}{2E_{1}}$$

$$\Leftrightarrow \frac{\mathrm{d}^{4}k_{1}}{(2\pi)^{3}} \delta(k_{1}^{2} - m_{t}^{2}) = \frac{\mathrm{d}^{3}\vec{k}_{1}}{(2\pi)^{3}} \frac{1}{2E_{1}}$$
(3.12)

We insert this relation into dPS<sub>2</sub> and integrate over  $d^4k_1$ , thereby eliminate one delta function:

$$dPS_{2} = \frac{d^{4}k_{1}}{(2\pi)^{3}} \delta(k_{1}^{2} - m_{t}^{2}) \frac{d^{3}\vec{k}_{2}}{(2\pi)^{3}} \frac{1}{2E_{2}} (2\pi)^{4} \delta^{(4)}(p_{1} + p_{2} - k_{1} - k_{2})$$

$$= \frac{1}{(2\pi)^{2}} \delta\left((p_{1} + p_{2} - k_{2})^{2} - m_{t}^{2}\right) \frac{d^{3}\vec{k}_{2}}{2E_{2}}.$$
(3.13)

We can use the definition of the partonic CM frame  $(\vec{p_1} + \vec{p_2}) = 0$  to further simplify the delta function; and we transform the integration over  $d^3\vec{k_2}$  into spherical coordinates:

$$d^{3}\vec{k}_{2} = |\vec{k}_{2}|^{2}d|\vec{k}_{2}|\sin\theta d\theta d\phi \qquad (3.14)$$

$$\delta\left((p_{1} + p_{2} - k_{2})^{2} - m_{t}^{2}\right) = \delta\left((p_{1} + p_{2})^{2} - 2(p_{1} + p_{2})k_{2} + k_{2}^{2} - m_{t}^{2}\right)$$

$$= \delta\left(s - 2\sqrt{s}E_{2}\right)$$

$$= \frac{1}{2\sqrt{s}}\delta\left(E_{2} - \frac{\sqrt{s}}{2}\right). \qquad (3.15)$$

The energy relationship  $E_2 = \sqrt{\vec{k}_2^2 + m_t^2}$  implies

$$\frac{\mathrm{d}E_2}{\mathrm{d}|\vec{k}_2|} = \frac{|\vec{k}_2|}{E_2} \,. \tag{3.16}$$

Plugging the relations 3.14, 3.15 and 3.16 into 3.13 we get

$$dPS_{2} = \frac{1}{(2\pi)^{2}} \frac{1}{2\sqrt{s}} \delta \left( E_{2} - \frac{\sqrt{s}}{2} \right) \frac{|\vec{k}_{2}|^{2}}{2E_{2}} d|\vec{k}_{2}| \sin \theta d\theta d\phi$$

$$= \frac{1}{(2\pi)^{2}} \frac{1}{2\sqrt{s}} \delta \left( E_{2} - \frac{\sqrt{s}}{2} \right) \frac{|\vec{k}_{2}|}{2} dE_{2} d\cos \theta d\phi.$$
(3.17)

Integrating over the Energy  $dE_2$  we can rewrite  $|\vec{k}_2|$  as follows:

$$|\vec{k}_2| = \sqrt{E_2^2 - m_t^2}$$

$$= \frac{\sqrt{s^2 - 4sm_t^2}}{2\sqrt{s}},$$
(3.18)

which leads to the final solution for the phase space element

$$dPS_2 = \frac{1}{16\pi^2} \frac{\sqrt{s^2 - 4sm_t^2}}{2s} d\cos(\theta) d\phi.$$
 (3.19)

Looking at the hadronic cross section (eq. 2.31), the incident flux F needs to be calculated as well. For a general collision between particles 1 and 2, the incident flux is given by [10]

$$F = |\vec{v}_1 - \vec{v}_2| \cdot 2E_1 \cdot 2E_2 .$$

For the given process, the flux simplifies to:

$$F = 2s. (3.20)$$

The final expression for the partonic cross section  $\sigma_{(ij\to kl)}$  can now be written as

$$\sigma_{(ij\to kl)} = \int_{-1}^{1} \frac{1}{32\pi} \frac{\sqrt{s^2 - 4sm_t^2}}{s^2} |M|^2 d\cos(\theta).$$
 (3.21)

## 4 Calculation of the Squared Matrix Element

The next step in calculating the hadronic cross section (eq. 2.30) is determining the squared matrix element. For this leading order calculation we consider all Feynman diagrams proportional to  $g_s^2$  that result in a  $t\bar{t}$ -pair in the final state. For the calculation of the squared matrix element we only look at gg-fusion<sup>2</sup>, where we look at the s-, t-, and u-channels. The matrix element is made up of the contributions for the three channels:  $M = M_s + M_t + M_u$ , which results in the squared matrix element:

$$|M|^{2} = (M_{s} + M_{t} + M_{u})(M_{s} + M_{t} + M_{u})^{\dagger}$$
  
=  $|M_{s}|^{2} + |M_{t}|^{2} + |M_{u}|^{2} + 2\operatorname{Re}(M_{s}M_{t}^{\dagger}) + 2\operatorname{Re}(M_{s}M_{u}^{\dagger}) + 2\operatorname{Re}(M_{t}M_{u}^{\dagger}).$ 

The relevant Feynman diagrams are listed in figure 3.

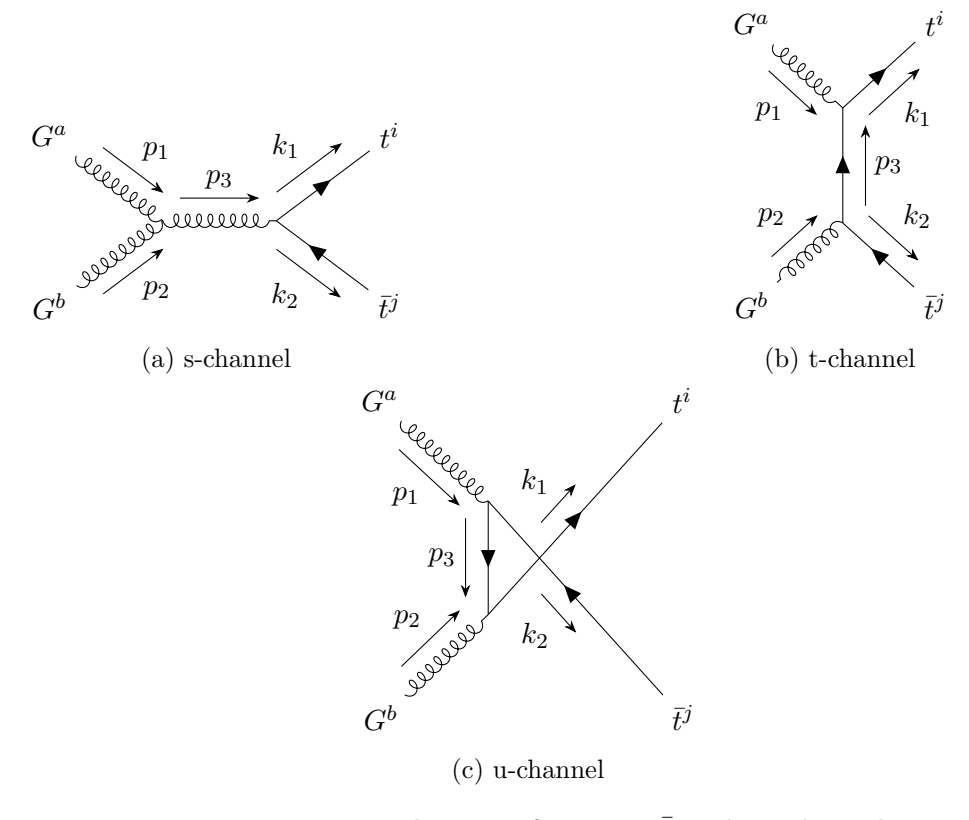


Figure 3: Feynman diagrams for  $gg \to t\bar{t}$  in three channels.

<sup>&</sup>lt;sup>2</sup>An explanation can be found in chapter 2.1

#### 4.1 S-Channel

The contribution of the s-channel results from the Feynman rules established in sec. 2.3:

$$M_{s} = \epsilon_{\alpha}^{\lambda_{1}}(p_{1})\epsilon_{\beta}^{\lambda_{2}}(p_{2}) \cdot \bar{u}^{s_{1}}(k_{1})(-i)gT_{ij}^{e}\gamma_{e}v^{s_{2}}(k_{2})$$

$$\times \frac{(-i)g^{\gamma\epsilon}\delta^{ce}}{p_{3}^{2}}(-g)f^{abc}(g_{\alpha\beta}(p_{1}-p_{2})_{\gamma}+g_{\beta\gamma}(p_{2}+p_{2})_{\alpha}+g_{\gamma\alpha}(-p_{3}-p_{1})_{\beta})$$

$$= \frac{g^{2}}{p_{3}^{2}}\epsilon_{\alpha}^{\lambda_{1}}(p_{1})\epsilon_{\beta}^{\lambda_{2}}(p_{2}) \cdot \bar{u}^{s_{1}}(k_{1})\gamma^{\gamma}v^{s_{2}}(k_{2}) \cdot T_{ij}^{c}f^{abc}$$

$$\times (g_{\alpha\beta}(p_{1}-p_{2})_{\gamma}+g_{\beta\gamma}(p_{2}+p_{2})_{\alpha}+g_{\gamma\alpha}(-p_{3}-p_{1})_{\beta}). \tag{4.1}$$

We further divide the contribution into four factors:

$$M_s = M_{s,color} M_{s,1} M_{s,2} M_{s,3} ,$$

$$M_{s,color} = T_{ij}^c f^{abc} ,$$

$$(4.2)$$

$$M_{s,1} = \frac{g^2}{p_3^2} \epsilon_{\alpha}^{\lambda_1}(p_1) \epsilon_{\beta}^{\lambda_2}(p_2) , \qquad (4.3)$$

$$M_{s,2} = \bar{u}^{s_1}(k_1)\gamma^{\gamma}v^{s_2}(k_2), \qquad (4.4)$$

$$M_{s,3} = g_{\alpha\beta}(p_1 - p_2)_{\gamma} + g_{\beta\gamma}(p_2 + p_2)_{\alpha} + g_{\gamma\alpha}(-p_3 - p_1)_{\beta}, \qquad (4.5)$$

to make the calculation clearer. We determine the adjoint of each factor:

$$M_{s,color}^{\dagger} = T_{ji}^d f^{abd} \,, \tag{4.6}$$

$$M_{s,1}^{\dagger} = \frac{g^2}{p_3^2} \epsilon_{\eta}^{\lambda_1 \star}(p_1) \epsilon_{\varphi}^{\lambda_2 \star}(p_2), \qquad (4.7)$$

$$M_{s,2}^{\dagger} = \bar{v}^{s_2}(k_2) \gamma^{\kappa} u^{s_1}(k_1) , \qquad (4.8)$$

$$M_{s,3}^{\dagger} = g_{\eta\varphi}(p_1 - p_2)_{\kappa} + g_{\varphi\kappa}(p_2 + p_2)_{\eta} + g_{\kappa\eta}(-p_3 - p_1)_{\varphi}. \tag{4.9}$$

To calculate  $|M_{s,color}|^2$ , we need to average over the  $(N^2 - 1)^2$  possible color combinations of the gluons and sum over all color combinations of the top quark and the anti-top quark. Using the relations 2.20,this results in:

$$|M_{s,color}|^{2} = M_{s,color} M_{s,color}^{\dagger}$$

$$= \frac{1}{(N^{2} - 1)^{2}} \sum_{c,d} \sum_{i,j} T_{ij}^{c} T_{ji}^{d} \sum_{a,b} f^{abc} f^{abd}$$

$$= \frac{1}{(N^{2} - 1)^{2}} \sum_{c,d} \sum_{i,j} T_{ij}^{c} T_{ji}^{d} T_{A} \delta^{cd}$$

$$= \frac{1}{(N^{2} - 1)^{2}} T_{A} \sum_{i} \sum_{d,j} T_{ij}^{d} T_{ji}^{d}$$

$$= \frac{1}{(N^{2} - 1)^{2}} T_{A} C_{F} \sum_{i} \delta^{ii}$$

$$= \frac{N}{2(N^{2} - 1)}. \tag{4.10}$$

To calculate the remaining squared factors, we need to sum over the spins of the topanti-top-quark pair and average over the polarization of the gluons. The calculations are as follows:

$$|M_{s,1}|^{2} = M_{s,1}M_{s,1}^{\dagger}$$

$$= \frac{g^{4}}{p_{3}^{4}} \frac{1}{4} \sum_{\lambda_{1},\lambda_{2}} \epsilon_{\alpha}^{\lambda_{1}}(p_{1}) \epsilon_{\beta}^{\lambda_{2}}(p_{2}) \epsilon_{\eta}^{\lambda_{1}\star}(p_{1}) \epsilon_{\varphi}^{\lambda_{2}\star}(p_{2})$$

$$\stackrel{(2.25)}{=} \frac{g^{4}}{4p_{3}^{4}} \left( \frac{p_{1\alpha}p_{2\eta} + p_{1\eta}p_{2\alpha}}{p_{1}p_{2}} - g_{\alpha\eta} \right) \left( \frac{p_{1\beta}p_{2\varphi} + p_{1\varphi}p_{2\beta}}{p_{1}p_{2}} - g_{\beta\varphi} \right) , \qquad (4.11)$$

$$|M_{s,2}|^{2} = M_{s,2}M_{s,2}^{\dagger}$$

$$\stackrel{(2.22)}{=} \sum_{s_{1},s_{2}} \bar{u}_{a}^{s_{1}}(k_{1})\gamma_{ab}^{\gamma}v_{b}^{s_{2}}(k_{2}) \cdot \bar{v}^{s_{2}}(k_{2}) c\gamma_{cd}^{\kappa}u^{s_{1}}(k_{1}) d$$

$$= \gamma_{ab}^{\gamma}(k_{2\lambda}\gamma^{\lambda} - m_{t})_{bc}\gamma_{cd}^{\kappa}(k_{1\sigma}\gamma^{\sigma} + m_{t})_{da}$$

$$= \operatorname{Tr}\left(\gamma^{\gamma}(k_{2\lambda}\gamma^{\lambda} - m_{t})\gamma^{\kappa}(k_{1\sigma}\gamma^{\sigma} + m_{t})\right)$$

$$= \operatorname{Tr}\left(\gamma^{\gamma}k_{2\lambda}\gamma^{\lambda}\gamma^{\kappa}k_{1\sigma}\gamma^{\sigma}\right) - m_{t}^{2}\operatorname{Tr}(\gamma^{\gamma}\gamma^{\kappa})$$

$$= 4k_{1\sigma}k_{2\lambda}(g^{\gamma\lambda}g^{\kappa\sigma} - g^{\gamma\kappa}g^{\lambda\sigma} + g^{\gamma\sigma}g^{\lambda\kappa}) - 4m_{t}^{2}g^{\gamma\kappa}$$

$$= 4(k_{1}^{\kappa}k_{2}^{\gamma} + k_{1}^{\gamma}k_{2}^{\kappa} - g^{\gamma\kappa}(k_{1} \cdot k_{2} + m_{t}^{2})) , \qquad (4.12)$$

$$|M_{s,3}|^{2} = M_{s,3}M_{s,3}^{\dagger}$$

$$= (g_{\alpha\beta}(p_{1} - p_{2})_{\gamma} + g_{\beta\gamma}(p_{2} + p_{2})_{\alpha} + g_{\gamma\alpha}(-p_{3} - p_{1})_{\beta})$$

$$\times (g_{\eta\varphi}(p_{1} - p_{2})_{\kappa} + g_{\varphi\kappa}(p_{2} + p_{2})_{\eta} + g_{\kappa\eta}(-p_{3} - p_{1})_{\varphi}) . \qquad (4.13)$$

From here we calculate the contribution to the squared matrix element  $|M_s|^2$  using Wolfram Mathematica [12] and the FeynCalc package [20].

$$|M_s|^2 = |M_{s,color}|^2 |M_{s,1}|^2 |M_{s,2}|^2 |M_{s,3}|^2$$

$$= g^4 \frac{2N}{N^2 - 1} \frac{(m_t^2 - t)(m_t^2 - u)}{s^2}$$
(4.14)

## 4.2 T-Channel

The contribution of the t-channel results from the Feynman rules as follows:

$$M_{t} = \left(\bar{u}^{s_{1}}(k_{1})(-i)gT_{im}^{a}\gamma^{\alpha}\epsilon_{\alpha}^{\lambda_{1}}(p_{1})\right) \cdot \frac{i(\not p_{3} + m_{t})}{p_{3}^{2} - m_{t}^{2}}\delta^{mn} \cdot \left(\epsilon_{\beta}^{\lambda_{2}}(p_{2})(-i)gT_{nj}^{b}\gamma^{\beta}v^{s_{2}}(k_{2})\right)$$

$$= \frac{-ig^{2}}{p_{3}^{2} - m_{t}^{2}} \cdot \epsilon_{\alpha}^{\lambda_{1}}(p_{1})\epsilon_{\beta}^{\lambda_{2}}(p_{2}) \cdot T_{im}^{a}T_{mj}^{b} \cdot \bar{u}^{s_{1}}(k_{1})\gamma^{\alpha}(\not p_{3} + m_{t})\gamma^{\beta}v^{s_{2}}(k_{2}). \tag{4.15}$$

The contribution is divided into three factors  $M_t = M_{t,1} \cdot M_{t,2} \cdot M_{t,color}$ , with the adjoint of each factor, respectively:

$$M_{t,1} = \frac{-ig^2}{p_3^2 - m_t^2} \cdot \epsilon_{\alpha}^{\lambda_1}(p_1) \epsilon_{\beta}^{\lambda_2}(p_2) \qquad M_{t,1}^{\dagger} = \frac{ig^2}{p_3^2 - m_t^2} \cdot \epsilon_{\sigma}^{\lambda_1 \star}(p_1) \epsilon_{\tau}^{\lambda_2 \star}(p_2) , \qquad (4.16)$$

$$M_{t,2} = \bar{u}^{s_1}(k_1) \gamma^{\alpha}(\not p_3 + m_t) \gamma^{\beta} v^{s_2}(k_2) \qquad M_{t,2}^{\dagger} = \bar{v}^{s_2}(k_2) \gamma^{\tau}(\not p_3 + m_t) \gamma^{\sigma} u^{s_1}(k_1) , \qquad (4.17)$$

$$M_{t,color} = T_{im}^a T_{mj}^b \qquad M_{t,color}^{\dagger} = T_{jk}^b T_{ki}^a . \qquad (4.18)$$

This is done analogously to the calculation of the s-channel to make the calculation clearer. Averaging over the polarization of the gluons, we get:

$$|M_{t,1}|^{2} = M_{t,1} M_{t,1}^{\dagger}$$

$$= \frac{g^{4}}{(p_{3}^{2} - m_{t}^{2})^{2}} \frac{1}{4} \sum_{\lambda_{1}, \lambda_{2}} \epsilon_{\alpha}^{\lambda_{1}}(p_{1}) \epsilon_{\beta}^{\lambda_{2}}(p_{2}) \epsilon_{\sigma}^{\lambda_{1} \star}(p_{1}) \epsilon_{\tau}^{\lambda_{2} \star}(p_{2})$$

$$= \frac{g^{4}}{4(p_{3}^{2} - m_{t}^{2})^{2}} \left( \frac{p_{1\alpha}p_{2\sigma} + p_{1\sigma}p_{2\alpha}}{p_{1}p_{2}} - g_{\alpha\sigma} \right) \left( \frac{p_{1\beta}p_{2\tau} + p_{1\tau}p_{2\beta}}{p_{1}p_{2}} - g_{\beta\tau} \right) . \tag{4.19}$$

We sum over the spins of the top- anti-top quark pair to get:

$$|M_{t,2}|^{2} = M_{t,2} M_{t,2}^{\dagger}$$

$$= \sum_{s_{1},s_{2}} \bar{u}^{s_{1}}(k_{1})_{a} \gamma_{ab}^{\alpha}(\not p_{3} + m_{t})_{bc} \gamma_{cd}^{\beta} v^{s_{2}}(k_{2})_{d} \cdot \bar{v}^{s_{2}}(k_{2})_{e} \gamma_{ef}^{\tau}(\not p_{3} + m_{t})_{fg} \gamma_{gh}^{\sigma} u^{s_{1}}(k_{1})_{h}$$

$$= (\not k_{1} + m_{t})_{ha} \cdot \gamma_{ab}^{\alpha}(\not p_{3} + m_{t})_{bc} \gamma_{cd}^{\beta} \cdot (\not k_{2} - m_{t})_{de} \cdot \gamma_{ef}^{\tau}(\not p_{3} + m_{t})_{fg} \gamma_{gh}^{\sigma}$$

$$= \operatorname{Tr}\left((\not k_{1} + m_{t}) \cdot \gamma^{\alpha}(\not p_{3} + m_{t}) \gamma^{\beta} \cdot (\not k_{2} - m_{t}) \cdot \gamma^{\tau}(\not p_{3} + m_{t}) \gamma^{\sigma}\right). \tag{4.20}$$

To calculate  $|M_{t,color}|^2$ , we average all possible color combinations similar to eq. 4.10, using relations 2.20:

$$|M_{t,color}|^{2} = M_{t,color} M_{t,color}^{\dagger}$$

$$= \frac{1}{(N^{2} - 1)^{2}} \sum_{m,k} \sum_{a,b} \sum_{i,j} T_{im}^{a} T_{mj}^{b} T_{jk}^{b} T_{ki}^{a}$$

$$= \frac{1}{(N^{2} - 1)^{2}} \sum_{m,k} \sum_{a,i} T_{im}^{a} C_{F} \delta_{mk} T_{ki}^{a}$$

$$= \frac{1}{(N^{2} - 1)^{2}} C_{F}^{2} N$$

$$= \frac{1}{4N}.$$
(4.21)

Using Mathematica [12], this results in the following for the contribution to the squared matrix element  $|M_t|^2$ :

$$|M_t|^2 = |M_{t,1}|^2 |M_{t,2}|^2 |M_{t,color}|^2$$

$$= -\frac{g^4}{2N(m_t^2 - t)^2 s^2} \left[ 4m^8 + 2m^6(t + 3u) - m^4(3t^2 + 24tu + 5u^2) + m^2(t^3 + 13t^2u + 9tu^2 + u^3) - tu(3t^2 + u^2) \right].$$
(4.22)

#### **U-Channel** 4.3

The contribution of the u-channel results from the Feynman rules as follows:

$$M_{u} = \frac{-ig^{2}}{p_{3}^{2} - m_{t}^{2}} \cdot \epsilon_{\alpha}^{\lambda_{1}}(p_{1})\epsilon_{\beta}^{\lambda_{2}}(p_{2}) \cdot T_{in}^{b} T_{nj}^{a} \cdot \bar{u}^{s_{1}}(k_{1})\gamma^{\beta}(p_{3}^{b} + m_{t})\gamma^{\alpha} v^{s_{2}}(k_{2}).$$
 (4.23)

The only difference compared to the t-channel is that the top and anti-top quarks are switched, which will lead to a contribution to the squared matrix element  $|M_u|^2$  where u and t switch places compared to  $|M_t|^2$  (eq. 4.22). Because of this, the calculations are similar to those for the t-channel and are performed in Mathematica [12]. This results in the final contribution to the squared matrix element  $|M_u|^2$  of the u-channel being the following:

$$|M_u|^2 = -\frac{g^4}{2N(m_t^2 - u)^2 s^2} \left[ 4m^8 + 2m^6(3t + u) - m^4(5t^2 + 24tu + 3u^2) + m^2(t^3 + 9t^2u + 13tu^2 + u^3) - tu(t^2 + 3u^2) \right].$$

$$(4.24)$$

#### Cross-Channels

As can be seen in equation 4.1, interference terms arise when calculating the total squared amplitude, which must also be taken into account. We will calculate the interference term  $\operatorname{Re}\left\{M_{t}M_{u}^{\dagger}\right\}=M_{t}M_{u}^{\dagger}$  in detail and keep the calculation for the other two terms short using Mathematica. We start by dividing the interference term into three different factors similar to those in the previous sections:

$$M_{t,1} = \frac{-ig^2}{t^2 - m_t^2} \cdot \epsilon_{\alpha}^{\lambda_1}(p_1) \epsilon_{\beta}^{\lambda_2}(p_2) \qquad M_{u,1}^{\dagger} = \frac{ig^2}{u^2 - m_t^2} \cdot \epsilon_{\sigma}^{\lambda_1 \star}(p_1) \epsilon_{\tau}^{\lambda_2 \star}(p_2) , \qquad (4.25)$$

$$M_{t,2} = \bar{u}^{s_1}(k_1) \gamma^{\alpha}(\not p_t + m_t) \gamma^{\beta} v^{s_2}(k_2) \qquad M_{u,2}^{\dagger} = \bar{v}^{s_2}(k_2) \gamma^{\sigma}(\not p_u + m_t) \gamma^{\tau} u^{s_1}(k_1) , \qquad (4.26)$$

$$M_{t,2} = \bar{u}^{s_1}(k_1)\gamma^{\alpha}(\not p_t + m_t)\gamma^{\beta}v^{s_2}(k_2) \qquad M_{u,2}^{\dagger} = \bar{v}^{s_2}(k_2)\gamma^{\sigma}(\not p_u + m_t)\gamma^{\tau}u^{s_1}(k_1), \quad (4.26)$$

$$M_{t,color} = T_{im}^a T_{mj}^b \qquad M_{t,color}^{\dagger} = T_{jk}^a T_{ki}^b . \tag{4.27}$$

Averaging over the polarizations of the gluons, we get the following:

$$M_{t,1}M_{u,1}^{\dagger} = \frac{g^4}{4(t-m_t^2)(u-m_t^2)} \left(\frac{p_{1\alpha}p_{2\sigma} + p_{1\sigma}p_{2\alpha}}{p_1p_2} - g_{\alpha\sigma}\right) \left(\frac{p_{1\beta}p_{2\tau} + p_{1\tau}p_{2\beta}}{p_1p_2} - g_{\beta\tau}\right) (4.28)$$

We sum over the spins of the top- and anti-top-quark pair to get:

$$M_{t,2}M_{u,2}^{\dagger} = \sum_{s_1, s_2} \bar{u}^{s_1}(k_1)_a \gamma_{ab}^{\alpha}(\not p_t + m_t)_{bc} \gamma_{cd}^{\beta} v^{s_2}(k_2)_d \cdot \bar{v}^{s_2}(k_2)_e \gamma_{ef}^{\sigma}(\not p_u + m_t)_{fg} \gamma_{gh}^{\tau} u^{s_1}(k_1)_h$$

$$= (\not k_1 + m_t)_{ha} \gamma_{ab}^{\alpha}(\not p_t + m_t)_{bc} \gamma_{cd}^{\beta}(\not k_2 - m_t)_{de} \gamma_{ef}^{\sigma}(\not p_u + m_t)_{fg} \gamma_{gh}^{\tau}. \tag{4.29}$$

To calculate the color term, we average all possible color combinations using relations 2.20:

$$M_{t,color} \cdot M_{u,color}^{\dagger} = \frac{1}{(N^2 - 1)^2} \sum_{m,k} \sum_{a,b} \sum_{i,j} T_{im}^a T_{mj}^b T_{jk}^a T_{ki}^b$$

$$= \frac{1}{4(N^2 - 1)^2} \sum_{m,k} \sum_{i,j} \left( \delta_{ik} \delta_{mj} - \frac{1}{N} \delta_{im} \delta_{jk} \right) \left( \delta_{mi} \delta_{jk} - \frac{1}{N} \delta_{mj} \delta_{ki} \right)$$

$$= \frac{1}{4(N^2 - 1)^2} \sum_{i,j} \left( \delta_{ij} \delta_{ji} - \frac{2}{N} \delta_{ii} \delta_{jj} + \frac{1}{N^2} \delta_{ij} \delta_{ij} \right)$$

$$= \frac{1}{4(N^2 - 1)^2} (N + \frac{1}{N} - 2N)$$

$$= -\frac{1}{4N(N^2 - 1)}. \tag{4.30}$$

Using Mathematica, the three terms are combined and the interference term for the t- and u-channel comes out as:

$$M_t M_u^{\dagger} = \frac{g^4}{2N(N^2 - 1)} \frac{(m_t^4 - tu)(8m_t^4 - 4m_t^2(t + u) + (t - u)^2)}{s^2(t - m_t^2)(u - m_t^2)}.$$
 (4.31)

We can calculate the remaining interference terms between the s- and t-channel and the s- and u-channel in a similar way:

$$M_s M_t^{\dagger} = -\frac{g^4 N}{2(N^2 - 1)} \frac{2m_t^6 - 2m_t^4 (t + 2u) + m^2 (t^2 + 4tu + u^2) - 2t^2 u}{s^2 (m^2 - t)}, \tag{4.32}$$

$$M_s M_u^{\dagger} = -\frac{g^4 N}{2(N^2 - 1)} \frac{2m_t^6 - 2m_t^4 (2t + u) + m^2 (t^2 + 4tu + u^2) - 2tu^2}{s^2 (m^2 - u)}.$$
 (4.33)

This results in the following squared matrix element using eq. 4.1:

$$|M|^{2} = -\frac{g^{4}}{2N(N^{2} - 1)s^{2}(m_{t}^{2} - t)^{2}(m_{t}^{2} - u)^{2}}$$

$$\times \left(6m_{t}^{8} - m_{t}^{4}(3t^{2} + 14tu + 3u^{2}) + m_{t}^{2}(t^{3} + 7t^{2}u + 7tu^{2} + u^{3}) - tu(t^{2} + u^{2})\right)$$

$$\times \left(-2m_{t}^{2}(N^{2} - 2)(t + u - m^{2}) + (N^{2} - 1)(t^{2} + u^{2}) - 2tu\right).$$

$$(4.34)$$

#### 5 Numerical Evaluation

After we have established the partonic cross section in equation 3.21 and the squared matrix element in equation 4.34, the hadronic cross section (eq. 2.30) can be evaluated numerically using Python. First, we define the integration limits and generate a series of evenly distributed random events. Then certain cuts are applied to the events to ensure consistency with the experimental data. After that the hadronic cross section can be calculated numerically using the Monte Carlo method. We create a set of unweighted events using the Hit-or-Miss Monte Carlo method, which are stored using the LHE data format [2]. Finally, two normalized differential cross sections as a function of rapidity the  $y_{CM}$  and the invariant mass  $m_{t\bar{t}}$  are calculated from the unweighted events and compared to experimental data in [13].

#### 5.1 Integration Bounds

First we need to generate a set of random and equally distributed points for the integration variables  $x_1$ ,  $x_2$  and  $\cos(\theta)$ . We start by determining the integration bounds for the integration over  $x_1$ ,  $x_2$  and  $\cos(\theta)$ .

$$\sigma_{had} = \sum_{i,j,k,l} \int \int dx_1 dx_2 f_i(x_1) f_j(x_2) \sigma_{(ij \to kl)}$$

Although the momentum fractions are defined to be between 0 and 1  $x_1, x_2 \in [0, 1]$ , the partons need to have enough energy to produce the final state, which leads to the confinement condition [14]:

$$m_{out}^2 \le s = x_1 x_2 S \quad \Leftrightarrow \quad \tau_0 \equiv \frac{4m_t^2}{S} \le x_1 x_2 \,,$$
 (5.1)

where  $m_{out} = 2m_t$  is the mass of the top quark pair and  $\tau_0$  is the threshold for the momentum fractions. This results in the following integration bounds for  $x_1$  and  $x_2$ :

$$\sigma_{had} = \int_{\tau_0}^1 dx_1 \int_{\frac{\tau_0}{x_1}}^1 dx_2 \sum_{i,j} f_i(x_1) f_j(x_2) \int_{-1}^1 \int_0^{2\pi} \frac{1}{16\pi^2} \frac{\sqrt{s^2 - 4sm_t^2}}{4s^2} |M|^2 d\cos(\theta) d\phi.$$

## 5.2 Generating Integration Variables

The random, uniformly distributed events should be generated so they sample the function in a way that accurately reflects its behavior. One can see in figure 6 that the cross section shows a big increase for small  $x_1$  and  $x_2$ . One possibility to account for this behavior is to substitute the momentum fraction logarithmic as follows:

$$\tilde{x}_1 = \ln(x_1), 
\tilde{x}_2 = \ln(x_2),$$
(5.2)

which ensures that more points are generated in this area. The distribution of generated points can be seen in figure 4, where the logarithmic distribution is clearly visible. Taking

into account the Jacobi determinant  $J = x_1x_2$  the hadronic cross section can be written as

$$\sigma_{had} = \int_{\ln(\tau_0)}^{0} d\tilde{x}_1 x_1 \int_{\ln(\frac{\tau_0}{x_1})}^{0} d\tilde{x}_2 x_2 \sum_{i,j} f_i(x_1) f_j(x_2)$$

$$\times \int_{-1}^{1} d\cos(\theta) \frac{2\pi}{16\pi^2} \frac{\sqrt{s^2 - 4sm_t^2}}{4s^2} |M|^2.$$
(5.3)

It must be taken into account that the variables s, t and u depend on  $x_1$ ,  $x_2$  and  $\cos \theta$  and must be transformed according to equations 3.11.

To evaluate the cross section numerically, a set of N random and equally distributed points is created for each variable. For  $\tilde{x}_1$  and  $\tilde{x}_2$ , one generates random numbers in the interval  $[\ln(\tau_0), 0]$  respectably. Displaying all points who fulfill the condition 5.1 on a logarithmic scale (fig. 4b) will show a linear boundary condition. To enhance efficiency, all generated points who did not pass condition 5.1 will be mirrored along the linear boundary, making them usable in further calculation. Summed up, we generate N random and equally distributed events for the variables:

$$\tilde{x}_1 \in [\ln(\tau_0), 0], 
\tilde{x}_2 \in [\ln(\tau_0), 0], 
\cos(\theta) \in [-1, 1],$$
(5.4)

with the confinement condition

$$ln(\tau_0) \le \tilde{x}_1 + \tilde{x}_2 \le 0.$$
(5.5)

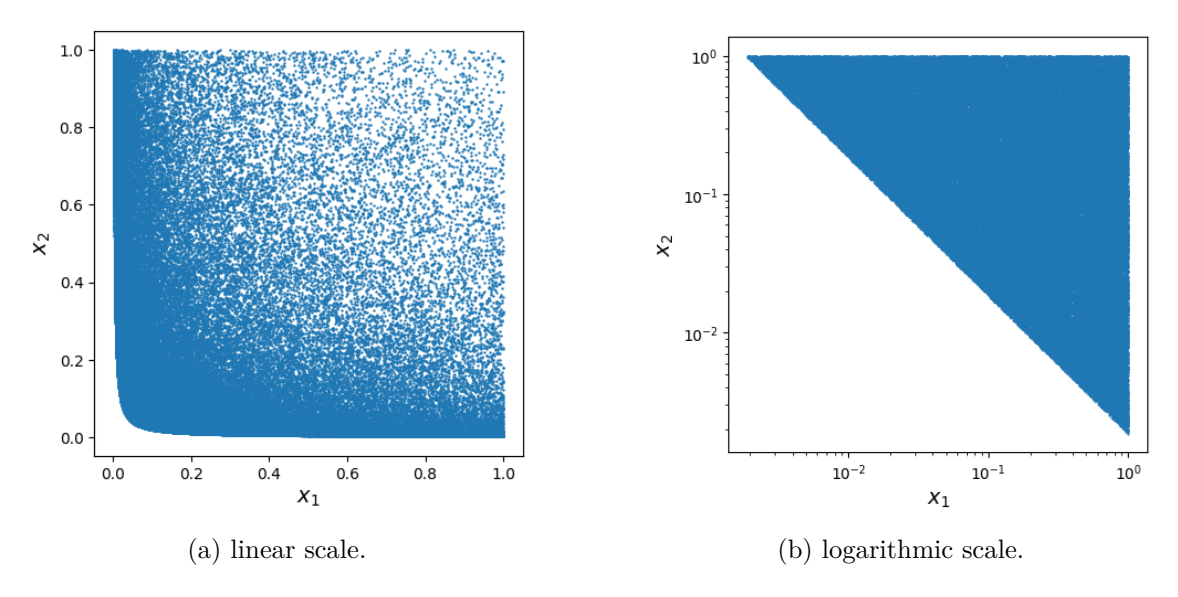


Figure 4: Distribution of the momentum fractions  $x_1$  and  $x_2$  displayed on linear and logarithmic scale. For better visibility only every hundredth event is shown.

#### 5.3 Cuts

To compare the theoretically calculated differential cross sections with experimental measurements [13], experimental limitations have to be taken into account. The first constrain is the rapidity of the CM system [5], the second constrain is given by the invariant mass of the top quark pair system [6]:

$$|y_{CM}| \le 2.5$$
,  
 $m_{t\bar{t}} \in [345, 1600] \,\text{GeV}$ . (5.6)

These constraints need to be addressed through cuts in the variables. The rapidity of the CM system is given by

$$y_{CM} = \frac{1}{2} \ln \left( \frac{x_1}{x_2} \right) \tag{5.7}$$

and the invariant mass is given by

$$m_{t\bar{t}}^2 = s = x_1 x_2 S. (5.8)$$

All variables who do not fulfill the conditions 5.6 are cut out and will not be used to calculate the cross section. Table 1 gives an overview on the cut conditions and lists the number of rejected and accepted events. Over all roughly 30% of the events got rejected.

Table 1: Overview on the number of rejected and accepted events with color code corresponding to fig. 5.

Cut Condition	Number of Events	Color
$m_{tar{t}} < m_{min}$	0	
$m_{t\bar{t}} > m_{max}$	2618324	
$ y_{CM}  > y_{cut}$	418903	
Number of rejected events	3037227	
Number of accepted events	6962773	
Total number of events	10000000	

Figure 5 shows the distribution of the rejected events on the left side and the distribution of the accepted events on the right side who will be used in the calculations later on. Blue points represent accepted events, where red and orange points represent events who got rejected because the invariant mass or the rapidity  $|y_{CM}|$  exceeded the experimental limitations. Discussing the effects of the cut conditions, one can see that the upper limit of the invariant mass cuts out events for large values of  $x_1$  and  $x_2$ , where as the limit on the rapidity is responsible for cutting out events with a large difference between the  $x_1$  and  $x_2$ values, which is in alignment to the condition 5.6. Both cut conditions lead to a symmetrical cut in the generated points for  $x_1$  and  $x_2$ . Looking at the  $\cos \theta$  distribution, we see that the upper limit of the invariant mass rejects events for large  $x_1$  and  $x_2$ , regardless of the value of  $\cos \theta$ . Similarly, the limitation of the rapidity  $|y_{CM}|$  is responsible for rejecting events for both very small and very large  $x_1$  and  $x_2$  regardless of the value of  $\cos \theta$ .

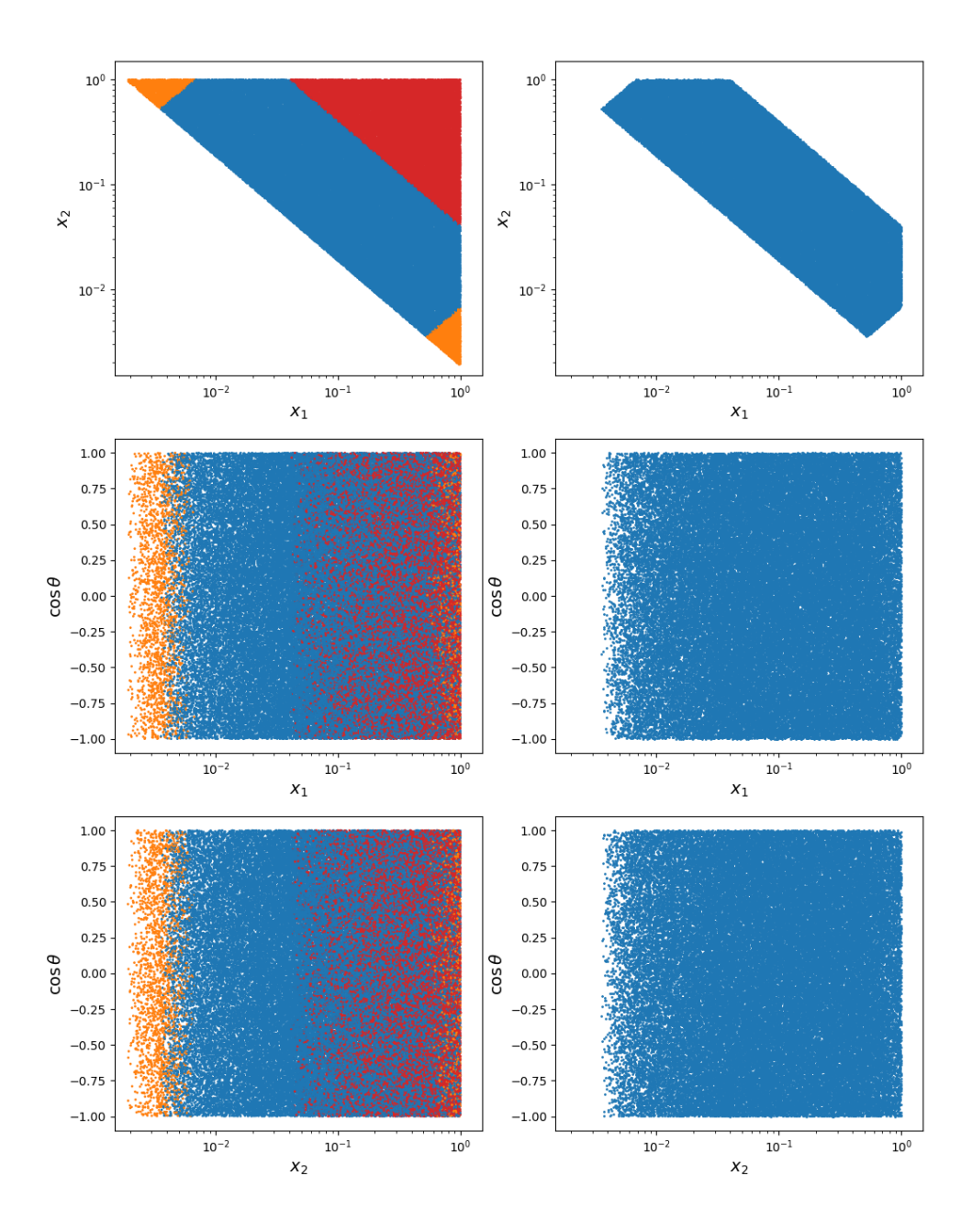


Figure 5: Distribution of all generated variables on left, where the color indicates the cut condition (see tab. 1). On the right are all points who passed the cuts. For better visibility only every hundredth event is shown.

#### 5.4 Evaluation of the Hadronic Cross Section

To evaluate the hadronic cross section in equation 5.3, the partonic distribution functions (PDF) need to be implemented. We use the PDF set "CT18NLO" [4], where one needs to take into account that each PDF includes a factor of x. At last, the Mandelstamm variables s, t and u who are used in the Matrix element need to be expressed through the variables  $x_1$ ,  $x_2$  and  $\cos \theta$  as shown in equations 3.11. Now, the hadronic cross section can be calculated using the Monte Carlo method as explained in section 2.5

$$I \approx \frac{V}{N} \sum_{k}^{N} \omega(x_1^{(k)}, x_2^{(k)}, \cos \theta^{(k)}),$$
 (5.9)

where we define the integral part as

$$\omega(x_1, x_2, \cos \theta) = x_1 x_2 \sum_{i,j} f_i(x_1) f_j(x_2) \frac{2\pi}{16\pi^2} \frac{\sqrt{s^2 - 4sm_t^2}}{4s^2} |M|^2,$$
 (5.10)

and the Volume V as

$$V = 2\frac{(0 - \ln(\tau_0))^2}{2} \frac{N_{accepted}}{N}.$$
 (5.11)

The Area over the variables  $x_1$  and  $x_2$  is a triangle and can be easily calculated. This area is multiplied by a factor of 2 derived from the variable  $\cos \theta$ . To account for the cuts in the events caused by the experimental limitations, the volume is multiplied by a ratio of accepted events to total events.

The 3D plots in figure 6 visualize the strength of the contribution to the cross-section for the variables  $x_1$ ,  $x_2$  and  $\cos \theta$ . The  $x_1$ - $x_2$  plane in the first figure is identical to the distribution shown in figure 5. In the brightly colored region the variables contibute most to the total cross section, which is the case for small values of  $x_1$  and  $x_2$  and for the regions around  $\cos \theta = \pm 1$ . The dark regions are kinematically possible but hardly produce any events. This aligns with the behavior of the PDF shown in figure 1, where it is shown that gluons carry the significant amount of momentum for small x. The hadronic cross section as shown in equation 5.3 can now be calculated to

$$\sigma_{had} = (175.79 \pm 0.10) \,\text{pb} \,.$$
 (5.12)

The uncertainty is given by the uncertainty of the Monte Carlo approximation and cannot be compared directly to uncertainties of experimental data. Inclusive top-quark pair production cross-section measurements at 8 TeV from the CMS collaboration [1] determine the cross section to be

$$\sigma_{t\bar{t}_{CMS}} = 244.9 \pm 1.4 \text{(stat.)}^{+6.3}_{-5.5} \text{(exp. + theo.)} \pm 6.4 \text{(lumi.)} \text{ pb}.$$
 (5.13)

The measurement has a relative deviation of about 25% from the LO prediction, which is acceptable considering the broad approximations assumed here. This leads to the conclusion that the neglected quark anti-quark annihilation and higher order corrections have significant impact on the total cross section which needs to be studied further in future calculations. Additionally the impact of the assumed energy scale Q needs to be studied and combined with uncertainties from the PDFs and MC method into an uncertainty for better comparison to the CMS data.

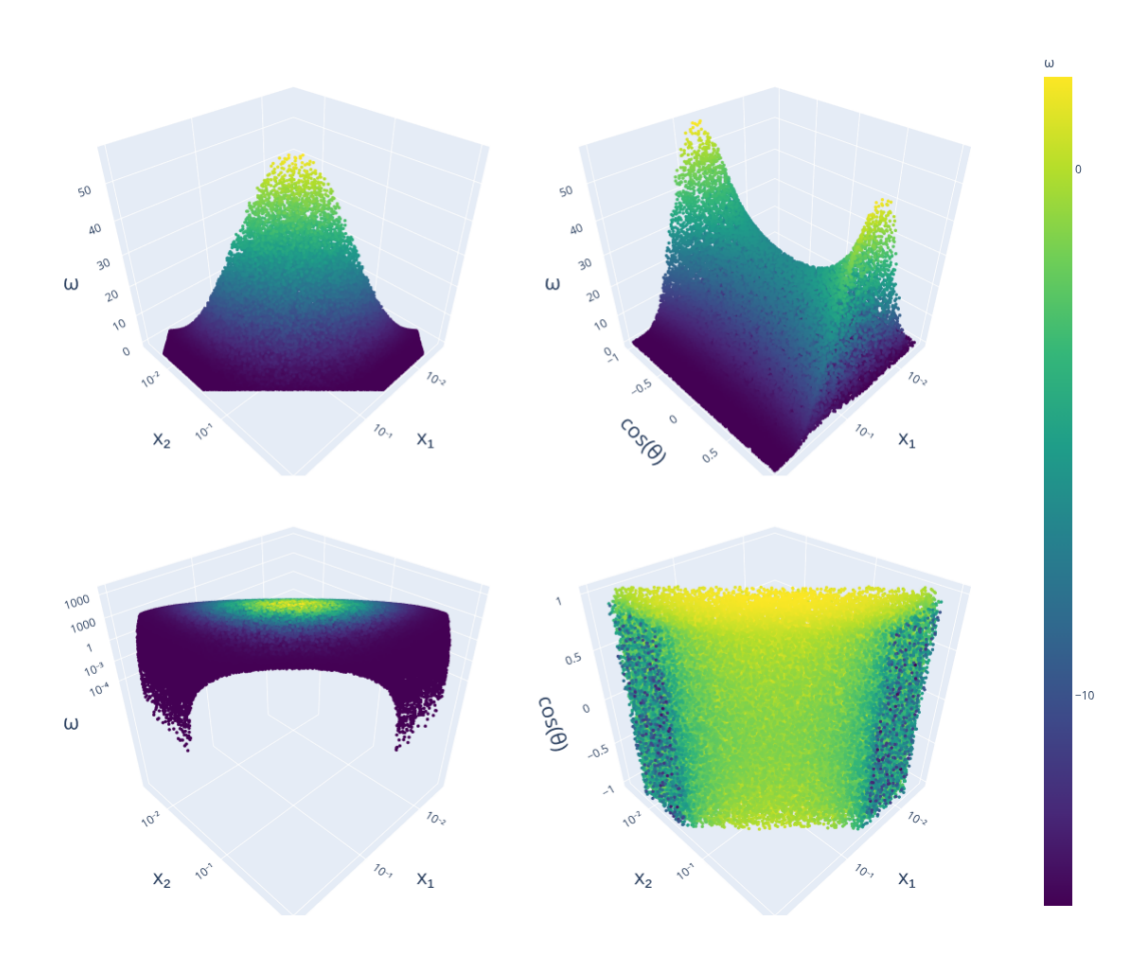


Figure 6: Three dimensional distribution of the integral part  $\omega$  (eq. 5.10) of the hadronic cross section as a function of  $x_1$ ,  $x_2$  and  $\cos \theta$ . The color codes the strength of the contribution to the cross-section.

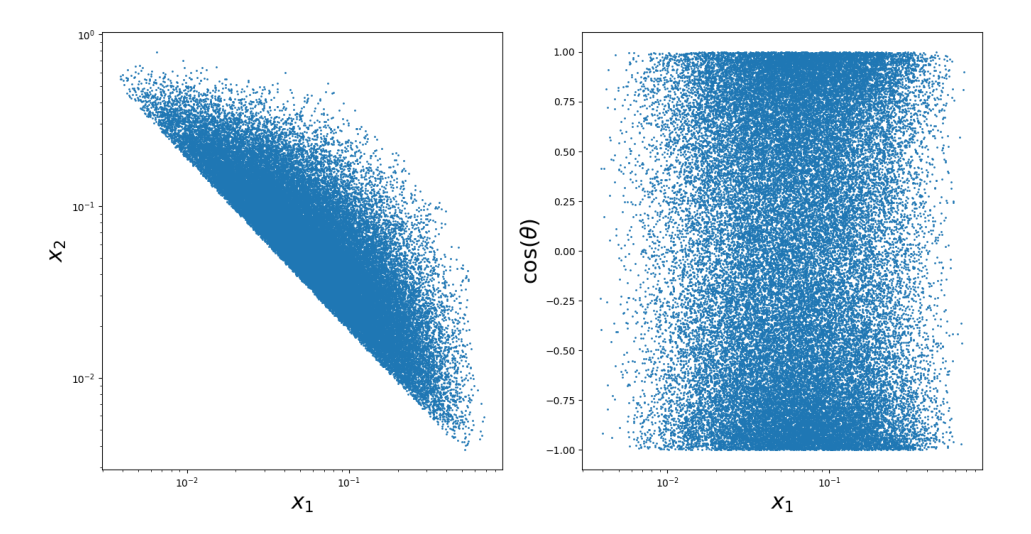


Figure 7: Distribution of accepted events after unweighting using Hit-or-Miss Monte Carlo. For better visibility only every tenth event is shown.

#### 5.5 Differential Cross Sections

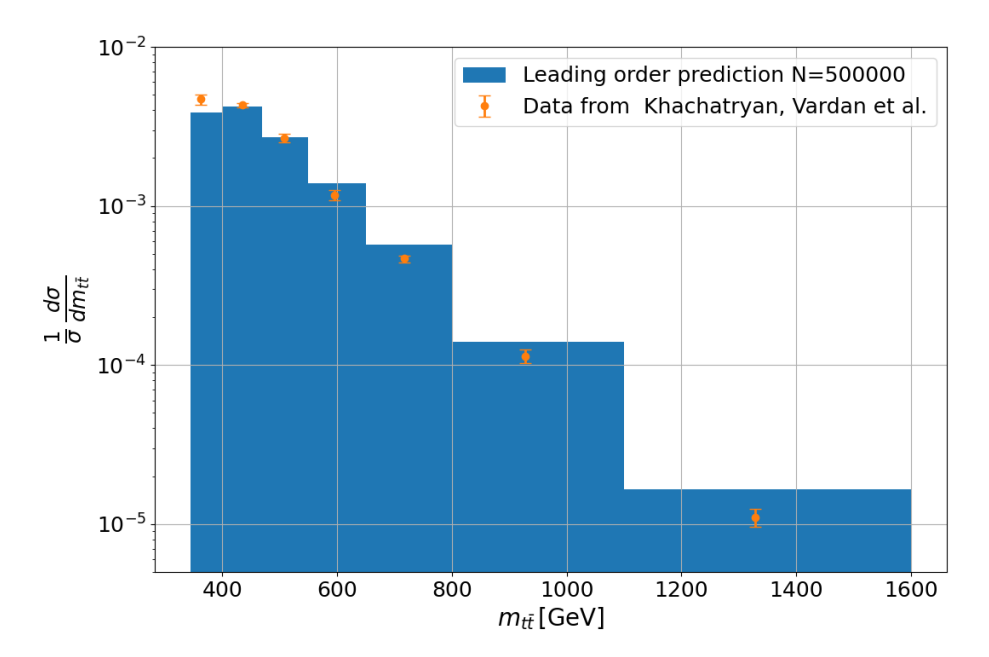
Compared to total cross sections, normalized differential cross sections can provide more information about the accuracy of the used boundaries and approximations, although it is not possible to make statements about the actual value of the cross section because of the normalization. We will compare the normalized differential  $t\bar{t}$  cross section as a function of the rapidity  $y_{t\bar{t}}$  and as a function of the invariant mass  $m_{t\bar{t}}$  of the top quark pair to the experimental data in [13], respectively the tables [5] and [6]. To calculate the differential cross sections, the Hit-or-Miss Monte Carlo Method is used in combination with the LHE data format [2]. We generate N=500000 unweighted events as described in section 2.5.1 and compute a LHE file using the unweighted events. For this number of events no relevant fluctuations can be observed while keeping the computation time manageable. The distribution of the accepted events for  $x_1$ ,  $x_2$  and  $\cos \theta$  can be seen in figure 7.

Comparing the unweighted distribution in figure 7 to figure 6, one can see the strength of the contribution to the cross section reflected in the distribution of the variables after unweighting. Small  $x_1$  and  $x_2$  are dominant in 7, and one can see that values for  $\cos \theta \approx \pm 1$  contribute more to the cross section compared to values closer to 0. This proves the unweighting method to be successful in reducing the size of generated events.

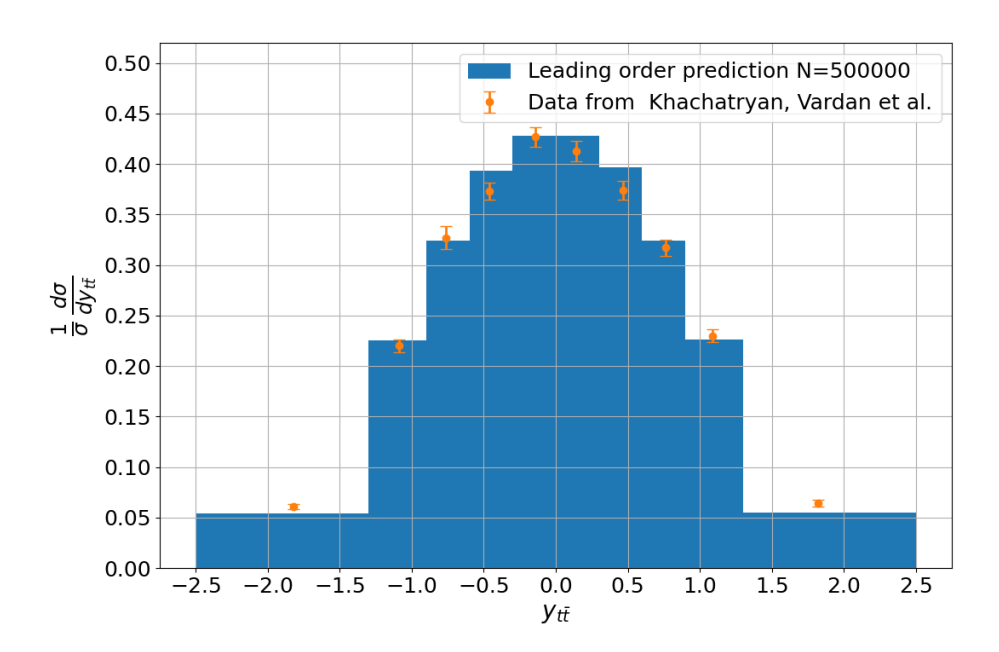
Next up we will analyze the differential cross sections and compare them to the data in [13]. The normalized cross section in each bin i of each observable X is determined through the relation:

$$\frac{1}{\sigma} \frac{\mathrm{d}\sigma_i}{\mathrm{d}X} = \frac{1}{\sum_i x_i} \frac{x_i}{\Delta_i^X},\tag{5.14}$$

where  $x_i$  represents the number of signal events measured in data in bin i, and  $\Delta_i^X$  is the bin width. The differential cross section is normalized by the sum of  $x_i$  over all bins [13].



(a) Normalized differential  $t\bar{t}$  production cross section as a function of  $m_{t\bar{t}}$ .



(b) Normalized differential  $t\bar{t}$  production cross section as a function of  $y_{CM}$ .

Figure 8: Normalized differential  $t\bar{t}$  production cross section as a function of  $m_{t\bar{t}}$  and  $y_{CM}$ . The leading order predictions are compared to experimental Data from [13].

Looking at the normalized differential  $t\bar{t}$  production cross section as a function of  $m_{t\bar{t}}$  in figure 8a, we observe multiple relevant discrepancies between the leading order prediction and the data. The prediction shows a peak for the  $m_{t\bar{t}}$  range  $(400-470)\,\mathrm{GeV}$ , whereas the data measures a steady incline for lower  $m_{t\bar{t}}$ . This is most likely caused by the multiple approximations done in this leading order calculation. The quark- anti-quark annihilation along with higher order corrections will most likely have a non negligible impact in the differential cross section. These terms have different effects on each bin, where it is hard to quantify the exact effect the corrections will have on each bin respectively. The leading order calculation predicts the measurements accurately in the range  $(400-550)\,\mathrm{GeV}$ , although overshooting significantly for  $m_{t\bar{t}} > 550\,\mathrm{GeV}$ . Overall the leading order calculation falsely predicts a peak for  $m_{t\bar{t}} \approx 435.3\,\mathrm{GeV}$ , but the general shape of the differential cross section for  $m_{t\bar{t}} > 550\,\mathrm{GeV}$  can be predicted.

Analyzing the normalized differential  $t\bar{t}$  production cross section as a function of  $y_{CM}$  in figure 8b, we see a roughly symmetrical plot around zero. The data shows the most prominent asymmetry at  $y_{CM} \approx 0$ , with a bigger differential cross section for rapidity in range [-0.3,0] compared to the range [0,0.3]. The leading order calculation predicts a symmetrical behavior, with statistical fluctuations appearing when less events N are created. The LO calculation predicts the overall shape of the differential cross section accurately, predicting a roughly symmetrical decline with higher rapidity. The prediction is accurate in ranges  $|y_{CM}| \in [0.6, 1.3]$ , while undershooting for bigger rapidity  $|y_{CM}| \in [1.3, 2.5]$  and generally overshooting in the range  $y_{CM} \in [-0.6, 0.6]$ . These discrepancies are again most likely caused by not including the quark- anti-quark annihilation and NLO and NNLO calculations.

## 6 Conclusion & Outlook

The hadronic cross section of  $t\bar{t}$ -production in proton-proton collisions at LHC is determined using a Monte Carlo framework for a leading order calculation. The phase-space element as well as the squared matrix element are calculated analytically partially supported by Mathematica. Because this process is gluon dominant, only gg-fusion is taken into account. For the numerical analysis a series of equally and random logarithmic distributed events are generated who fulfill the confinement condition, given by the minimum energy required to produce the final state. Additional cuts for the rapidity of the CM system and the invariant mass of the top quark pair system are introduced to account for experimental limitations. The distribution of the events are displayed in figure 5, where both cut conditions result in symmetrical cuts, cutting out events with large values of  $x_1$  and  $x_2$  as well as rejecting events for large differences between  $x_1$  and  $x_2$ . The three dimensional visualization of the cross section is shown in figure 6, where we see that small values of  $x_1$  and  $x_2$  have the biggest impact to the CS, combined with values around  $\cos \theta \approx \pm 1$ . This confirms the gluon dominance of this process. The cross section from our LO calculation

$$\sigma_{had} = (175.79 \pm 0.10) \,\mathrm{pb}$$

compared to measurements done by CMS collaboration

$$\sigma_{t\bar{t}CMS} = 244.9 \pm 1.4 \text{(stat.)} ^{+6.3}_{-5.5} \text{(exp. + theo.)} \pm 6.4 \text{(lumi.)} \text{ pb}$$

shows a relative deviation of about 25% from the CMS measurement. The uncertainty listed in our results derives from the uncertainty of the Monte Carlo method and cannot be compared to experimental uncertainties. This deviation is acceptable considering the approximations assumed here. We assume that the discrepancy is caused by neglecting the quark- anti-quark annihilation and NLO or NNLO corrections.

A series of unweighted events is generated using the Hit-or-Miss Monte Carlo method from which LHE-format events are created. These are used to calculate normalized differential  $t\bar{t}$  production cross sections as a function of  $m_{t\bar{t}}$  and  $y_{CM}$ , shown in figure 8. The LO calculation predict the overall shape of the differential CS, although incorrectly predicting a peak at  $m_{t\bar{t}} \approx 435.3\,\text{GeV}$  and failing to predict a slight asymmetrical distribution in the normalized differential CS as a function of  $y_{CM}$ . The neglect of the quark-antiquark annihilation and NLO and NNLO corrections are assumed to be responsible for the discrepancies, having complex influence on each bin independently.

This leading order calculation lays out a solid foundation for further improvement. Future work should include quark anti-quark annihilation and current state of the art corrections to study how these effect the accuracy of our predictions. Additionally, future work should focus on quantifying an uncertainty by varying the energy scale Q, including the uncertainties from PDFs and combine these in some way with the uncertainty from the MC method.

In conclusion, this thesis gave me valuable insights in the working methods of theoretical particle physics. I learned a lot about the theoretical framework and gained experience in analytical and numerical calculation methods. We show that for this process even LO calculations predict experimental measurements in the correct order of magnitude, which forms a foundation for future improvements.

## A Appendix

#### Gell-Mann Matrices

In analogy to the Pauli matrices for SU(2), the eight Gell-Mann matrices  $\lambda^a$  (a = 1, ..., 8) span the Lie algebra of SU(3). They are defined as the following  $3 \times 3$  Hermitian and traceless matrices:

$$\lambda^{1} = \begin{pmatrix} 0 & 1 & 0 \\ 1 & 0 & 0 \\ 0 & 0 & 0 \end{pmatrix}, \quad \lambda^{2} = \begin{pmatrix} 0 & -i & 0 \\ i & 0 & 0 \\ 0 & 0 & 0 \end{pmatrix}, \quad \lambda^{3} = \begin{pmatrix} 1 & 0 & 0 \\ 0 & -1 & 0 \\ 0 & 0 & 0 \end{pmatrix},$$

$$\lambda^{4} = \begin{pmatrix} 0 & 0 & 1 \\ 0 & 0 & 0 \\ 1 & 0 & 0 \end{pmatrix}, \quad \lambda^{5} = \begin{pmatrix} 0 & 0 & -i \\ 0 & 0 & 0 \\ i & 0 & 0 \end{pmatrix}, \quad \lambda^{6} = \begin{pmatrix} 0 & 0 & 0 \\ 0 & 0 & 1 \\ 0 & 1 & 0 \end{pmatrix},$$

$$\lambda^{7} = \begin{pmatrix} 0 & 0 & 0 \\ 0 & 0 & -i \\ 0 & i & 0 \end{pmatrix}, \quad \lambda^{8} = \frac{1}{\sqrt{3}} \begin{pmatrix} 1 & 0 & 0 \\ 0 & 1 & 0 \\ 0 & 0 & -2 \end{pmatrix}.$$
(A.1)

They satisfy the normalization condition

$$Tr(\lambda^a \lambda^b) = 2 \,\delta^{ab},\tag{A.2}$$

and the commutation relations

$$[\lambda^a, \lambda^b] = 2if^{abc}\lambda^c, \tag{A.3}$$

where  $f^{abc}$  are the totally antisymmetric SU(3) structure constants. The Gell-Mann matrices are widely used in QCD to represent the color degrees of freedom of quarks and gluons.

#### **Dirac Matrices**

The Dirac matrices  $\gamma^{\mu}$  are defined as a set of  $4\times 4$  matrices that satisfy the Clifford algebra

$$\{\gamma^{\mu}, \gamma^{\nu}\} \equiv \gamma^{\mu} \gamma^{\nu} + \gamma^{\nu} \gamma^{\mu} = 2g^{\mu\nu} \mathbb{I}_4, \tag{A.4}$$

where the brackets represent the anticommutator,  $g^{\mu\nu}$  is the metric tensor of Minkowski space and  $\mathbb{I}_4$  is the  $4\times 4$  identity matrix. The matrices can also be written using the  $2\times 2$  identity matrix  $\mathbb{I}_2$ 

$$\gamma^0 = \begin{pmatrix} \mathbb{I}_2 & 0 \\ 0 & -\mathbb{I}_2 \end{pmatrix}, \qquad \gamma^i = \begin{pmatrix} 0 & \sigma^i \\ -\sigma^i & 0 \end{pmatrix}, \quad i = 1, 2, 3, \tag{A.5}$$

with  $\sigma^i$  the Pauli matrices. One can impose the relations

$$(\gamma^0)^\dagger = \gamma^0 \qquad (\gamma^\mu)^\dagger = -\gamma^\mu = \gamma^0 \gamma^\mu \gamma^0 \quad \text{for } \mu = 1, 2, 3.$$

The Feynman slash notation is defined by

$$\phi := \gamma^{\mu} a_{\mu}$$

for any four vector a.

#### Relevant Identities

The following identities follow from the fundamental anticommutation relation and are used in the calculations:

$$\gamma^{\mu}\gamma_{\mu} = 4\mathbb{I}_4 \tag{A.6}$$

$$\gamma^{\mu}\gamma^{\nu}\gamma_{\mu} = -2\gamma^{\nu} \tag{A.7}$$

$$\gamma^{\mu}\gamma^{\nu}\gamma^{\rho}\gamma_{\mu} = 4g^{\nu\rho}\mathbb{I}_4 \tag{A.8}$$

#### **Trace Relations**

The cyclic property of the trace is fundamental:

$$Tr(AB) = Tr(BA). (A.9)$$

It is invariant under circular shifts and its a linear mapping:

$$Tr\{ABCD\} = Tr\{BCDA\} = Tr\{CDAB\} = Tr\{DABC\}$$
(A.10)

$$Tr{A + B} = Tr{A} + Tr{B}$$
(A.11)

$$Tr\{cA\} = c Tr\{A\} \tag{A.12}$$

for all square matrices A and B and all scalars  $c \in \mathbb{C}$ .

For the Dirac matrices, important trace identities are:

$$Tr(\gamma^{\mu}) = 0, \tag{A.13}$$

$$Tr(\gamma^{\mu}\gamma^{\nu}) = 4g^{\mu\nu},\tag{A.14}$$

$$\operatorname{Tr}(\gamma^{\mu}\gamma^{\nu}) = 4g^{\mu\nu}, \tag{A.14}$$

$$\operatorname{Tr}(\gamma^{\mu}\gamma^{\nu}\gamma^{\rho}\gamma^{\sigma}) = 4\left(g^{\mu\nu}g^{\rho\sigma} - g^{\mu\rho}g^{\nu\sigma} + g^{\mu\sigma}g^{\nu\rho}\right). \tag{A.15}$$

Traces with an odd number of Dirac matrices vanish:

$$\operatorname{Tr}(\gamma^{\mu_1}\gamma^{\mu_2}\cdots\gamma^{\mu_{2n+1}})=0. \tag{A.16}$$

#### Metric Tensor

The metric tensor  $g^{\mu\nu}$  defines the scalar product in Minkowski space. In the mostly-minus convention,

$$g^{\mu\nu} = \begin{pmatrix} 1 & 0 & 0 & 0 \\ 0 & -1 & 0 & 0 \\ 0 & 0 & -1 & 0 \\ 0 & 0 & 0 & -1 \end{pmatrix},\tag{A.17}$$

it allows for raising and lowering of Lorentz indices:

$$A_{\mu} = g_{\mu\nu}A^{\nu}, \qquad A^{\mu} = g^{\mu\nu}A_{\nu}.$$
 (A.18)

Contractions with the metric also reproduce the Kronecker delta:

$$g^{\mu\nu}g_{\nu\rho} = \delta^{\mu}_{\ \rho}.\tag{A.19}$$

## References

- [1] G. Aad et al. "Combination of inclusive top-quark pair production cross-section measurements using ATLAS and CMS data at  $\sqrt{s}=7$  and 8 TeV". In: *Journal of High Energy Physics* 2023.7 (July 2023). issn: 1029-8479. doi: 10.1007/jhep07(2023)213. url: http://dx.doi.org/10.1007/JHEP07(2023)213.
- [2] J. Alwall et al. "A standard format for Les Houches Event Files". In: Computer Physics Communications 176.4 (Feb. 2007), pp. 300-304. issn: 0010-4655. doi: 10. 1016/j.cpc.2006.11.010. url: http://dx.doi.org/10.1016/j.cpc.2006.11.010.
- [3] M. Beneke et al. Top Quark Physics. 2000. arXiv: hep-ph/0003033 [hep-ph]. url: https://arxiv.org/abs/hep-ph/0003033.
- [4] Andy Buckley et al. "LHAPDF6: parton density access in the LHC precision era". In: The European Physical Journal C 75.3 (Mar. 2015). issn: 1434-6052. doi: 10.1140/epjc/s10052-015-3318-8. url: http://dx.doi.org/10.1140/epjc/s10052-015-3318-8.
- [5] CMS Collaboration. "Table 36" of "Measurement of the differential cross section for top quark pair production in pp collisions at sqrt(s) = 8 TeV" (Version 1). HEPData (dataset). https://doi.org/10.17182/hepdata.68516.v1/t36. 2016.
- [6] CMS Collaboration. "Table 39" of "Measurement of the differential cross section for top quark pair production in pp collisions at sqrt(s) = 8 TeV" (Version 1). HEPData (dataset). https://doi.org/10.17182/hepdata.68516.v1/t39. 2016.
- [7] CMS Collaboration. Measurement of the differential cross section for top quark pair production in pp collisions at sqrt(s) = 8 TeV. HEPData (collection). https://doi.org/10.17182/hepdata.68516. 2016.
- [8] Giorgio Cortiana. "Top-quark mass measurements: Review and perspectives". In: Reviews in Physics 1 (2016), pp. 60-76. issn: 2405-4283. doi: https://doi.org/10.1016/j.revip.2016.04.001. url: https://www.sciencedirect.com/science/article/pii/S2405428316300028.
- [9] Benjamin Grinstein. "Introductory lectures on QCD". In: 2nd CERN-CLAF School of High Energy Physics. June 2003, pp. 27–56.
- [10] Francis Halzen and Alan Martin. Quarks & Leptons: An introductory course in modern particle physics. New York, USA: John Wiley & Sons, 1984.
- [11] W. Hollik. Quantum field theory and the Standard Model. 2010. arXiv: 1012.3883 [hep-ph]. url: https://arxiv.org/abs/1012.3883.
- [12] Wolfram Research Inc. *Mathematica*, *Version 14.3*. Champaign, IL, 2025. url: https://www.wolfram.com/mathematica.
- [13] Vardan Khachatryan et al. "Measurement of the differential cross section for top quark pair production in pp collisions at  $\sqrt{s}=8\,\text{TeV}$ ". In: Eur. Phys. J. C 75.11 (2015), p. 542. doi: 10.1140/epjc/s10052-015-3709-x. arXiv: 1505.04480 [hep-ex].

- [14] Karol Kovařík. Drell-Yan and Jets. private notes. 2023.
- [15] Karol Kovařík. HITCHHIKER'S GUIDE TO RENORMALIZATION. unpublished, 2021.
- [16] Michelangelo L Mangano. "Introduction to QCD". In: (2000). doi: 10.5170/CERN-1999-004.53. url: https://cds.cern.ch/record/454171.
- [17] Andreas Papaefstathiou. "How-to: write a parton-level Monte Carlo particle physics event generator". In: Eur. Phys. J. Plus 135.6 (2020), p. 497. doi: 10.1140/epjp/s13360-020-00499-1. arXiv: 1412.4677 [hep-ph].
- [18] Bogdan Povh et al. Particles and Nuclei. An Introduction to the Physical Concepts.
   Graduate Texts in Physics. 2015. isbn: 978-3-662-46320-8, 978-3-662-49583-4, 978-3-662-46321-5. doi: 10.1007/978-3-662-46321-5.
- [19] Jakob Schwichtenberg. *Physics from Symmetry*. Undergraduate Lecture Notes in Physics. Springer, 2018. isbn: 978-3-319-19201-7, 978-3-319-66630-3, 978-3-319-88288-8, 978-3-319-66631-0. doi: 10.1007/978-3-319-66631-0.
- [20] Vladyslav Shtabovenko, Rolf Mertig, and Frederik Orellana. "FeynCalc 9.3: New features and improvements". In: Computer Physics Communications 256 (Nov. 2020), p. 107478. issn: 0010-4655. doi: 10.1016/j.cpc.2020.107478. url: http://dx.doi.org/10.1016/j.cpc.2020.107478.

## **Declaration of Academic Integrity**

I hereby confirm that this thesis, entitled
is solely my own work and
that I have used no sources or aids other than the ones stated. All passages in my thesis for
which other sources, including electronic media, have been used, be it direct quotes or content
references, have been acknowledged as such and the sources cited. I am aware that plagiarism
is considered an act of deception which can result in sanction in accordance with the
examination regulations.
(date, signature of student)
I consent to having my thesis cross-checked with other texts to identify possible similarities
and to having it stored in a database for this purpose.
I confirm that I have not submitted the following thesis in part or whole as an examination
paper before.
(date, signature of student)